



“Forest carbon sequestration mapping and economic quantification infusing MLPnn-Markov chain and InVEST carbon model in Askot Wildlife Sanctuary, Western Himalaya”



Pragati Verma ^{a,*}, Azizur Rahman Siddiqui ^b, Nitesh Kumar Mourya ^c, Ahanthem Rebika Devi ^d

^a Department of Economics, University of Allahabad, Prayagraj, Uttar Pradesh, India

^b Department of Geography, University of Allahabad, Prayagraj, Uttar Pradesh, India

^c GeoCatalog – Institute of Research and Geoinformatics, New Delhi, India

^d University School of Environment Management, Guru Gobind Singh Indraprastha University, New Delhi, India

ARTICLE INFO

Keywords:

Carbon mapping
Machine learning
Net present value (NPV)
Sensitivity analysis
InVEST model
Markov chain

ABSTRACT

Due to the expeditious rise in anthropogenic activities and rapid extractive pressure, protected areas in the Indian Himalayan Region (IHR) are experiencing significant losses in ecological diversity and a substantial decline in the potential for carbon sequestration and climate change mitigation. The quantification of carbon sequestration and the understanding of its corresponding economic gain/loss are crucial for raising strict preservative concerns in protected areas with rich ecological and economic values. Transitions in land use land cover (LULC) trajectories from historical to future scenarios impact the dynamics of carbon storage and sequestration in terrestrial ecosystems. The present study extends a comprehensive 40-year (1995–2035) assessment of carbon mapping (gain/loss) as well as an economic approximation of carbon sequestration in the Askot Wildlife Sanctuary (AWLS), Western Himalaya, using satellite data. This investigation presents a novel hybrid approach by infusing machine learning algorithms and a spatial-temporal technique-based MLPnn-Markov chain model for future LULC simulation with the InVEST model that incorporates carbon mapping and economic valuation. The results show that among all the land use classes, dense forest has the highest carbon density; however, it exhibits a decreasing trend from 1995 (5,695,878.41 Mg/ha) to 2035 (4,378,439.81 Mg/ha). The economic quantification of carbon sequestration was performed by applying sensitivity analysis combined with different carbon prices and discount rates from 2020 to 2035. The observed outcomes reveal significant economic losses due to rapid forest cover decline, as indicated by a negative net present value (NPV) ranging from a minimum of ~US\$ -8 million to a maximum of ~US\$ -53 million. This study develops a valuable database by providing evidence-based decision-making and guidance for the sustainable preservation of ecosystems in the Western Himalayas and similar regions worldwide, where forest carbon sequestration is of paramount importance. The findings of the study suggest sound provisions for the conservation of forested landscapes and the development of efficient voluntary and regulatory carbon trading markets to achieve stability in forest carbon stocks. In doing so, this interdisciplinary approach addresses the growing imperative of integrating ecological and economic aspects in the context of biodiversity conservation and climate change mitigation.

1. Introduction

Forests are vital for sustaining life on earth by furnishing essential organic infrastructure, preserving biodiversity, purifying air and water, supporting local livelihoods, and mitigating climate change. Concurrently, they serve as natural barriers against geophysical phenomena such as landslides, soil erosion, and avalanches (Mansourian et al.,

2009). Nearly 1/3rd of the CO₂ (2.6 billion tonnes of C) emitted from fossil fuel combustion is sequestered by forests every year (IUCN, 2021). In order to maintain the forests' benefits, it is necessary to protect them from destructive anthropogenic interventions. Recent research (Harris et al., 2021) has published observations on global annual forest GHG emissions and removals between the years 2001–2019 by integrating ground and satellite data. The findings reveal that deforestation and

* Corresponding author.

E-mail address: pragati20verma@gmail.com (P. Verma).

forest degradation lead to gross global emissions of approximately $8.1 \pm 2.5 \text{ GtCO}_2\text{eq year}^{-1}$ (mean \pm s.d.), and gross removals amount to $-15.6 \pm 49 \text{ GtCO}_2\text{eq year}^{-1}$. When balancing these opposing fluxes, the net global forest carbon sink is approximately $-7.6 \pm 49 \text{ GtCO}_2\text{eq year}^{-1}$. However, there are significant uncertainties in these estimates due to spatial-temporal variations worldwide. As reported by Soares-Filho et al. (2010), 27% of global net forest carbon (C) sinks lie in protected areas (PAs), which act as a valuable instrument for climate change mitigation, especially when combined with control and command management practices (Mansourian et al., 2009).

The Indian Himalayan Region (IHR), recognised as one of the world's 36 biodiversity hotspots (Dangwal et al., 2022) due to its ecological richness, accounts for a range of PA networks represented by 99 wildlife sanctuaries, 28 national parks, and 5 biosphere reserves, covering $70,074.54 \text{ km}^2$ geographical area of IHR (Bargali et al., 2022; Rawal and Dhar, 2001). Forests are the dominant landscape feature in the IHR, occupying 41% of its geographical area. Among these forests, very dense forests make up 16.9%, moderate forests comprise 45.7%, and the remaining 37.7% consist of open forests (Negi, 2018). The forests in IHR store about 3000 million tonnes of C, representing nearly 40% of the total forest carbon sequestration (FCS) in India (Dangwal et al., 2022; Rawal et al., 2021). The annual FCS in the whole IHR is about 65 million tonnes, encompassing aboveground biomass (AGB) and forest soil (FS) (Singh, 2007; Tolangay and Moktan, 2020). The estimated economic value of this sequestered carbon in AGB + FS is approximately US\$ 843 million (Singh, 2007). Studies have reported a growth in the volume of carbon storage in Himalayan forests, increasing from 2.7 to 3.3 Mg, with an annual increment of 0.6 Mg of C, corresponding to 2.2 Mg of CO₂ (Bisht et al., 2022).

Apart from extending a huge carbon sink and contributing economic value, Himalayan forests dispense numerous tangible benefits, i.e., fuel wood, timber, fibre, fodder, medicines, and other non-timber forest products. They are also integral to the environment, culture, economy, and history of the country (Negi, 2018). These forests cover 24.2 million hectares in IHR, out of which 30% is distorted due to anthropogenic disturbances such as overgrazing, cutting, and lopping (Bisht et al., 2022; FSI, 2019). This degradation is driven by factors such as high population growth, high poverty ratio, and limited resources for livelihood (Akash et al., 2022). As a result of escalating human pressures, developmental activities, and natural distortions, the Himalayan forests are depleting at a rate of $0.36 \text{ km}^2/\text{year}$ (Rawat and Sharma, 2012), causing a drastic alteration in terms of forest structure, function, and species composition (Daman Singh et al., 2022; Sagar et al., 2003), which is leading to a loss of carbon storage capacity. Therefore, to conserve and restore the forest ecosystem on a global and local scale, the United Nations has declared the present decade (2021–2030) as the Decade of Ecosystem Restoration. Under this initiative, the degraded forest land will be restored, ensuring the conservation of biological variability, supply of forest products, and enhancement of carbon sequestration for climate change mitigation (Rawal et al., 2021). Aligned with these conservation efforts, India committed to the Bonn Challenge Pledge in 2015—the most ambitious pledge from Asia. The country aims to restore 13 million hectares of degraded and deforested land by 2020, with a further goal to rehabilitate an additional 8 million hectares by 2030¹. India is also working as an important stakeholder in the implementation of the REDD+ mechanism, which was adopted at COP 19 as the Warsaw Framework for REDD+ (WFR) under the United Nations Framework Convention on Climate Change (UNFCCC). It aims to promote sustainable forest management and conservation and increase forest carbon storage capacity in developing countries while reducing GHG emissions (MoEFCC, 2018). Apart from this, in order to protect the rare virtues of the Himalayan ecosystem, the Government of India (GOI) has launched a specific mission known as the National

Mission for Sustaining the Himalayan Eco-system. This is one of eight missions under the National Action Plan for Climate Change (NAPCC). Moreover, the National Mission for a Green India under NAPCC also puts special emphasis on the forestry sector for enhancing the resilience and adaptation capacity of forests against climate change (Negi, 2018).

There is abundant scope to utilise forests in the Himalayan region as carbon sinks and to develop carbon markets by involving all the stakeholders, including local communities. The use of financial incentives as payment for ecosystem services can help prevent the rapid conversion of forest landscapes into other land uses (Miteva et al., 2012; Naime et al., 2020). Mechanisms like cap-and-trade and trading of carbon credits promote carbon markets by adding monetary value to ecosystem services (Pache et al., 2021; Wayburn, 2009). Nevertheless, these markets still require some modifications and smooth functioning for widespread implementation (Katila and Puustjärvi, 2003). To achieve this, the externalities (positive/negative) generated by ecosystems must be considered in decision-making to avoid market failure resulting from inefficient (under or over) allocation of resources (Katila and Puustjärvi, 2003; Verma and Ghosh, 2023). There are also inherent risks and uncertainties involved in measuring the monetary value of carbon associated with carbon additionality, leakage, and permanence (Sedjo and Sohngen, 2012). Additionally, spatio-temporal changes in LULC significantly influence the outcome of FCS and its economic assessment (Adelisardou et al., 2022; Momo and Devi, 2022). Apparently, there are various challenges in the quantification of the economic value of FCS due to the complex structure and dynamic nature of forest ecosystems, which include several ecological and economic components (Omara et al., 2003). This underscores an urgent need for suitable carbon mapping software and accurate simulation models, which can provide sufficient information to narrow down the gap between real world decision-making and scientific knowledge in the efficient management of ecosystems (Nguyen et al., 2020; Ouyang et al., 2016). In recent advances, several LULC simulation models, including the MLP neural network-Markov chain (MLPnn-MC) model (Nasiri et al., 2019; Vass and Elofsson, 2016; Vinayak et al., 2020), SD-CLUE-S model (Liang et al., 2017), Logistic-CA-MC model (Guan et al., 2019), FLUS model (Liang et al., 2018), SLEUTH model (Kumar and Agrawal, 2022), PLUS model (Tao et al., 2023) and others, integrated with carbon mapping and valuation model, i.e., InVEST (Integrated Valuation of Ecosystem Services and Tradeoffs), have emerged as reliable techniques providing promising results for stakeholders and decision-makers.

There are a host of studies integrating various simulation and carbon assessment models (Abd El-Hamid and Hafiz, 2022; Liang et al., 2017; Tao et al., 2023) to investigate variation in carbon stock (CS) in terrestrial ecosystems as a response to the change in LULC pattern. Furthermore, various studies (Avtar et al., 2022; Babbar et al., 2021; Gupta et al., 2017; Yu et al., 2020) have performed economic valuation of carbon sequestration in terms of net present value (NPV), linking with future LULC prediction modelling and carbon change assessment. Whereas, infrequent literature has conducted the economic quantification of carbon sequestration specifically within forests (Chu et al., 2019; Nguyen et al., 2020; Pache et al., 2021). Thus, there still remains a huge scope for the assessment of carbon in forest ecosystems as a natural capital to maintain the balance of global C cycle.

Addressing this gap, in the present communication, we propose a novel approach to estimate the economic value of FCS in terms of NPV (US\$) at different social cost of carbon (SSC) set as carbon prices and discount rates by integrating MLPnn-MC and InVEST models in AWLS. The MLPnn-MC model is used to forecast the future LULC map based on the historical transition matrix, and subsequently, the InVEST model is applied for carbon mapping and valuation of FCS, utilising both ecological and economic data.

The main objectives of this study are enumerated as follows:

- (1) prepare LULC maps for AWLS and perform the change analysis for 1995, 2008, and 2020;

¹ <https://www.bonnchallenge.org/>

- (2) Simulate and validate LULC maps for 2020 and 2035 using IDRISI Selva 17.0 software;
- (3) perform carbon mapping using the InVEST model to investigate the dynamics of carbon sequestration over time;
- (4) apply sensitivity analysis while calculating the NPV for FCS in US \$ at different carbon prices and discount rates.

2. Materials and methods

2.1. Study area

Askot Wildlife Sanctuary (AWLS), established in 1986, is situated in the north of Pithoragarh, a district in the Kumaun region of Uttarakhand, Western Himalayas. The sanctuary sprawls over 600 km² and lies between the coordinates of longitudes 81°01'53"E and 80°16'25"E and latitudes 29°46'45"N and 30°27'45"N at 5412 ft elevation above sea level (Fig. 1). This landscape has three main watersheds: the Kali and East Dhauli rivers originate from this place, and the Gori Ganga streams through it. The annual climate of the study area encompasses three notable seasons: summer (March–June), rainy season (July–September), and winter (November–February). The climate, soil diversity, and unique topography of the region comprise lush vegetation, diverse species, and habitats (Samant et al., 2006). The landscape possesses three major forest ecozones: sub-alpine forest, temperate broadleaved forest, and sub-tropical forest (Bisht et al., 2023).

The sanctuary is under extreme threat due to increasing human encroachment and human-animal conflicts. To protect the ecology and biodiversity, AWLS has been announced as an Eco-Sensitive Zone (ESZ) in December 2021, according to the gazette released by the Union Environment Ministry, which is a buffer zone at the extent of highly-protected areas. Now the sanctuary sprawl has been reduced to only 454.65 km² from the original 600 km².

2.2. Data sources and acquisition

The information about the datasets used in the study for spatial-temporal mapping is delineated in Table 1. The satellite data, Landsat 05 Thematic Mapper (TM), was acquired for 1995 and 2008, and Landsat 08 Operational Land Image (OLI) and Thermal Infrared Sensor (TIRS) were retrieved for 2020 from the USGS Earth Explorer website². Each image is cloud-free and has a 30 m spatial resolution, projection to UTM Zone 44 N, WGS84 datum, 145/039 path and rows, and 1071/903 columns and rows. Landsat 05 TM images consist of 7 spectral bands, where bands 1 to 5 and 7 have a 30 m spatial resolution and band 6 (thermal infrared) has a 120 m resolution. Landsat 08 OLI TIRS carries two sensors: OLI and TIRS, and has 11 bands. Bands 1 to 7 and 9 have a 30 m resolution, band 8 (panchromatic) has a 15 m resolution, and bands 10 and 11 are collected at 100 m. In this study, for LULC preparation, only a 6-band combination, 1 to 5, and 7 bands are used for Landsat 05, and a 7-band combination, 1 to 7, is used for Landsat 08. In addition to this, some supplementary data is also produced as a driver variable to be used in the simulation modelling. SRTM (Shuttle Radar Topography Mission) 1 Arc – Second Global DEM and slope data are extracted from the USGS Earth Explorer portal. Geographical data for roads, waterways, buildings, land use, and places are obtained from OSM (Open Street Map)³.

2.3. Research design and data processing

The research workflow of the study is organised into three stages, viz., data processing and classification, change detection and prediction, and valuation of C sequestration. At the first stage, pre-processing of

satellite data, such as band composite, georeferencing, and study area extraction, is performed to prepare the LULC maps for change detection and trend analysis. Further, some GIS functions and digital image processing methods are employed in ArcGIS 10.7.1 and ERDAS IMAGINE 2015, respectively, for LULC classification and accuracy assessment. At the second stage, the prepared LULC maps are converted into binary format in order to easily import and run them into IDRISI Selva 17.0 software for future prediction. At the third and last stage, historical and future carbon mapping are performed to observe the carbon stock changing pattern. After that, the economic value of carbon sequestration is estimated in US\$. Hence, this section presents a brief overview of the entire method, technique, and processing incorporated in the study, as replicated in Fig. 2. More details about models and methods are elaborated on in the succeeding sections.

2.4. LULC classification and accuracy assessment

RGB composite Landsat images for 1995, 2008, and 2020 are used to create the LULC map of AWLS (Fig. 3). Before implementing any approach to classification (supervised/unsupervised), understanding the complexity of the study area is very essential (Shivakumar and Rajashekharadhy, 2018). Various band combinations were examined to understand the spectral separability of various land features, where a few classes overlapped due to equal spectral – radiometric values. A supervised classification technique has been performed in ERDAS IMAGINE software by applying the Maximum Likelihood Classifier (MLC), which is based on a parametric classification algorithm and requires careful spectral pattern recognition for high-quality training sample extraction, also known as signature collection. To perform this function, a 5, 4, 1 RGB band combination for LANDSAT 05 (which provides a ‘natural-like’ rendition) and a 7, 5, 3 RGB band combination for LANDSAT 08 (which provides natural colour with atmospheric removal) are employed for separating the land cover features into different LULC classes. More than one training sample was used to show a specific class. During the supervised classification procedure, all the collected signatures saved in the signature editor, containing various information about the defined LULC classes, are used for the classification process. The satellite image was then classified into ten classes, viz., Dense Forest, Open Forest, Agriculture, Grassland, Degraded Land, Barren Land, Water Bodies, Snow Cover, Built-up, and Sand Bar (Fig. 3). Further, the classes were validated by high-resolution Google Earth Pro satellite images, and a few classes were re-coded for the actual class. To assess the reliability of the classified image, an accuracy assessment is executed as an important post-classification step in which a reference dataset is used to compare the classified image to determine the level of accuracy. Stratified random sampling is adopted in ERDAS IMAGINE, and then 500 sample points were created in the study area. Kappa analysis, a discrete multivariate technique, is used to calculate producer’s accuracy, user’s accuracy, overall accuracy, and overall kappa statistics to find the accuracy and reliability of the LULC maps produced (Table 2).

2.5. Model description

2.5.1. MLPnn-MC modelling

MLPnn-MC modelling integrates the multi-layer perceptron (MLP) algorithm and Markov chain, which unravels robust future LULC simulation (Gebresellase et al., 2023; Nasiri et al., 2019). The novelty of this model lies in the fact that it utilises deep machine learning to learn the model in automated mode in less calibration time through complex, multivariate, and non-linear relationships to create several transitions and predict unseen data within the model at a single time by comprehending the hidden relationships (Kumar and Agrawal, 2023). MLP is the most prevalent machine learning algorithm in ANN (Artificial Neural Network) modelling (Alla et al., 2021; Band et al., 2020), which uses back propagation (BP) or the reverse method of automatic

² <https://earthexplorer.usgs.gov/>.

³ www.openstreetmap.org/#map=4/21.84/82.79

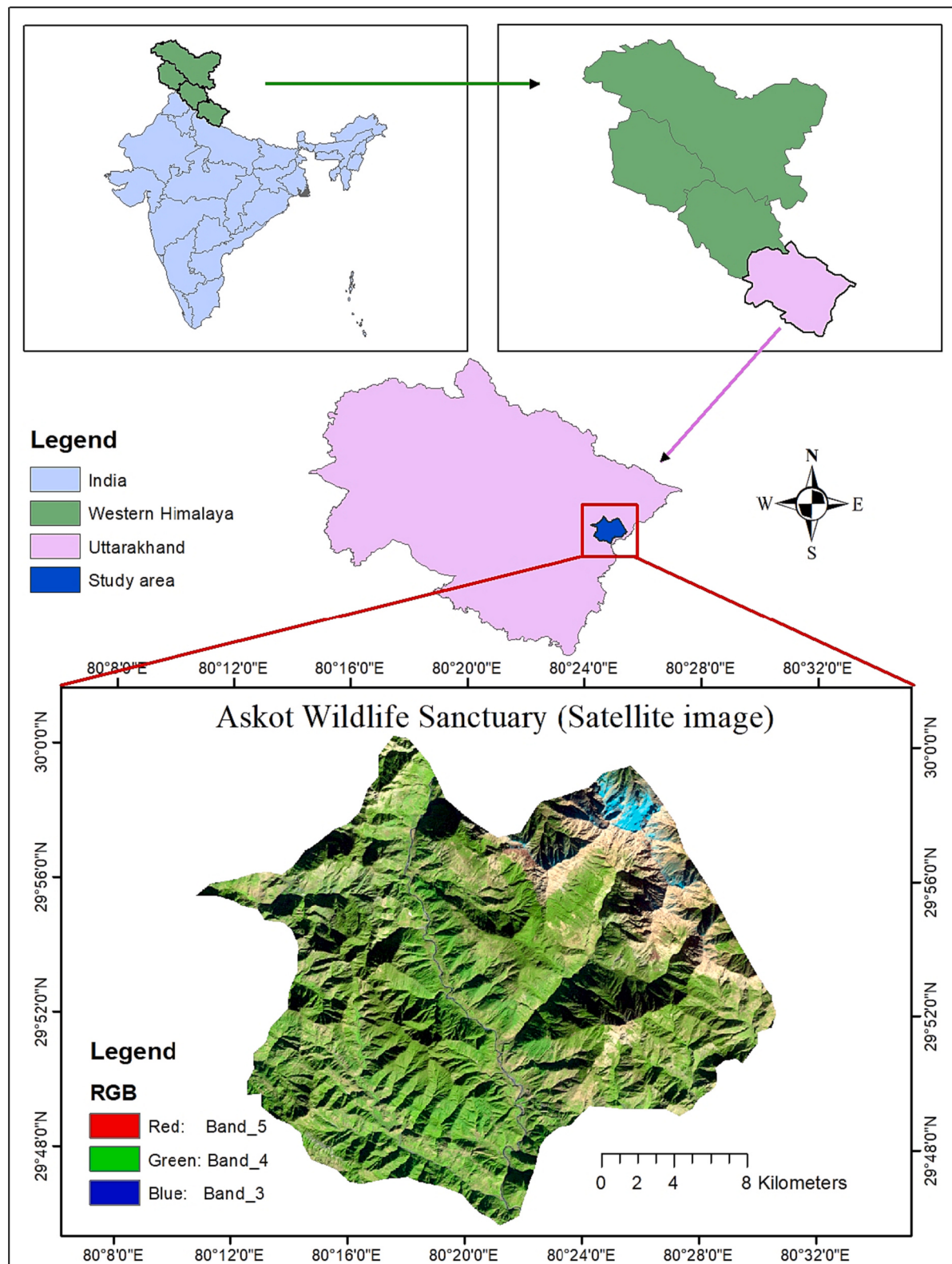


Fig. 1. Location map.

differentiation as a feedforward propagation (FP) algorithm to train the neural networks by employing supervised learning based on stochastic gradient descent (SGD). Backward pass always improves the efficiency of MLP neural networks. Generally, MLP consists of three main layers of nodes: an input layer, an output layer, and one or more hidden layers in-between them (Kumar and Agrawal, 2023). Apart from the input layer,

each layer is a neuron that operates on non-linear activation function, such as sigmoid. These neurons are organised in such a way that the networks are directed only from lower to upper layers, and the neurons within the same layer are independent. Input data is provided to the input node, processed through the hidden layers in an iterative manner, and the output layer provides the pattern classification. The Markov

Table 1

Raster and supplementary data information used in the study.

S. No.	Data type	Source	Date Acquired (yyyy/mm/dd)	Path and rows	Resolution	Columns and rows	Bands
Raster information used for LULC preparation							
1.	Landsat 05 TM	USGS Earth Explorer	1995/12/15	145/039	30 m	1071/903	6
2.	Landsat 05 TM	USGS Earth Explorer	2008/12/18	145/039	30 m	1071/903	6
3.	Landsat 08 OLI TIRS	USGS Earth Explorer	2020/12/19	145/039	30 m	1071/903	7
Supplementary Data							
1.	DEM	SRTM USGS	–	–	30 m	–	–
2.	Slope	SRTM USGS	–	–	30 m	–	–
3.	Distance from road	OSM data	–	–	–	–	–
4.	Distance from waterway	OSM data	–	–	–	–	–
5.	Distance from buildings	OSM data	–	–	–	–	–
6.	Distance from landuse	OSM data	–	–	–	–	–
7.	Distance from places	OSM data	–	–	–	–	–

chain exhibits stochastic “memory-less” behaviour, implying that the random transition of an event from the present state to the future state under certain probable conditions depends solely on the existing event and time elapsed (Gebresellase et al., 2023; Mahfuz, 2021). The Markov property of “forgetting” the previous event is referred to as memoryless property.

The mathematical representation of the Markov model for future prediction is indicated below (Choudhari, 2013; Hua, 2017), where p_{ij} denotes the transition matrix, signifying transition FROM (X_t) TO (X_{t+1}) under conditional probability.

$$X_{t+1} = p_{ij} \cdot X_t \quad (1)$$

$$p_{ij} = \begin{bmatrix} p_{11} & \cdots & p_{1n} \\ \vdots & \ddots & \vdots \\ p_{n1} & \cdots & p_{nn} \end{bmatrix}$$

$$0 \leq p_{ij} \geq 1, i, j = 1, 2, \dots, n \quad (2)$$

In the present study, this model was implemented within the Land Change Modeler (LCM) module of IDRISI Selva 17.0, which provides a consolidated platform with access to GIS and remote sensing data to investigate the spatial-temporal change in LULC (Kumar and Agrawal, 2023; Mirici et al., 2017; Vinayak et al., 2020). LCM carries a hybrid/fusion approach as it combines properties of machine learning through MLP with the merits of both Markov chain (MC) and cellular automata (CA) (Asadi et al., 2022; Mirici et al., 2017; Sabree Ali et al., 2020). Markov chain is an empirical statistics-based model (Marko et al., 2016) that calculates likelihood of pixel transition quantitatively from one class to another in the form of transition matrix. However, this approach lacks location knowledge (Arsanjani et al., 2013; Asadi et al., 2022; Shafizadeh Moghadam and Helbich, 2013), which is supplemented by the spatially-explicit “bottom-up” approach-based CA dynamic model (Faichia et al., 2020). The CA model simulates transition in location over a period of time (Hegde et al., 2007; Itami, 1994) using the following formula:

$$X_{t+1} = f(X_t, N) \quad (3)$$

where: X = possible states; N = all neighbouring cells; and f = transition function.

By integrating the models, the quantitative transition calculated by the Markov model can now be spatially geo-referenced through the CA model (Arsanjani et al., 2013; Hua, 2017; Marko et al., 2016). In the present study, multi-temporal land use maps from 1995, 2008, and 2020 have been used to project the complex and dynamic trajectory of future LULC for the year 2035. To initiate the LCM model, it requires earlier and later landcover images. Further, it runs across several steps of the model, namely: change and spatial trend analysis; preparation of sub-transition model; selection of driver variables and running the MLPnn parameters to generate the transition potential maps; execution of the Markov chain model to generate a transition matrix for future

prediction; and finally, performing validation of the simulated landscape.

2.5.2. InVEST carbon model

“InVEST” – (Integrated Valuation of Ecosystem Services and Trade-offs) is an open source suite of 25 different spatially-explicit integrated models developed by NatCap (Natural Capital Project, 2022), Stanford University, to map, quantify, and value ecosystem services (Bera et al., 2022; Chu et al., 2019; Hoque et al., 2021). The InVEST carbon storage and sequestration (CS & S) model (v3.12.0) is used in this study to estimate the C stock (static) and amount of C sequestration over time (dynamic) in each cell of the landscape parcel based on four C-density pools: aboveground biomass (AGB), belowground biomass (BGB), soil organic matter (SOM), and dead organic matter (DOM). The C-densities in each C pool were further aggregated for all land use categories to accumulate the value of $C_{storage}$ across the landscape. $C_{k(x,y)}$ is carbon value for (x,y) grid-cell within land use type k that can be formulated as:

$$C_{k(xy)} = A \times (C_{AGB_{k(x,y)}} + C_{BGB_{k(x,y)}} + C_{SOM_{k(x,y)}} + C_{DOM_{k(x,y)}}) \quad (4)$$

where, A is area (in ha) of each grid-cell and C_{AGB} , C_{BGB} , C_{SOM} , and C_{DOM} are the values of C-density (Mg/ha) in each pool. Hence, $C_{storage}$ and $C_{sequestration}$ across the entire land parcel can be calculated as:

$$C_{storage} = \sum_{k=1}^n C_{k(x,y)} \quad (5)$$

($k = 1, 2, \dots, n$), where n is no.of LULC type

$$C_{sequestration} = C^{future} - C^{current} \quad (6)$$

In Eq. (6), C^{future} and $C^{current}$ are the static C stocks in future and current periods, respectively. The required data to run the model were current and future LULC maps and biophysical table in CSV format containing the columns: ‘C_above’, ‘C_below’, ‘C_soil’, and ‘C_dead’ (Table 3). The C-pool data were acquired from the InVEST user guide (Adelisardou et al., 2022) and a meta-analysis of various published documents (Liang et al., 2017; Piyathilake et al., 2022; Tao et al., 2023), assuming that C-densities in each pool have not changed over the different scenarios (from 1995 to 2035). Finally, the $C_{storage}$ is calculated in dense forest, open forest, agriculture, grassland, barren land, water bodies, and built-up areas to monitor and project the dynamics of CS & S in AWLS during 1995–2035. The other land use classes, such as degraded land, snow cover, and sand bar, are reported to contain less biomass, so the C value was assumed to be 0 (Momo and Devi, 2022). Once the C stock (CS) is calculated, the InVEST model is processed to produce the map of CS & S in each grid-cell (in Mg/pixel) for the entire study area.

In the next process, the InVEST model conducts an economic valuation of C sequestration, not storage, since market prices consider only C

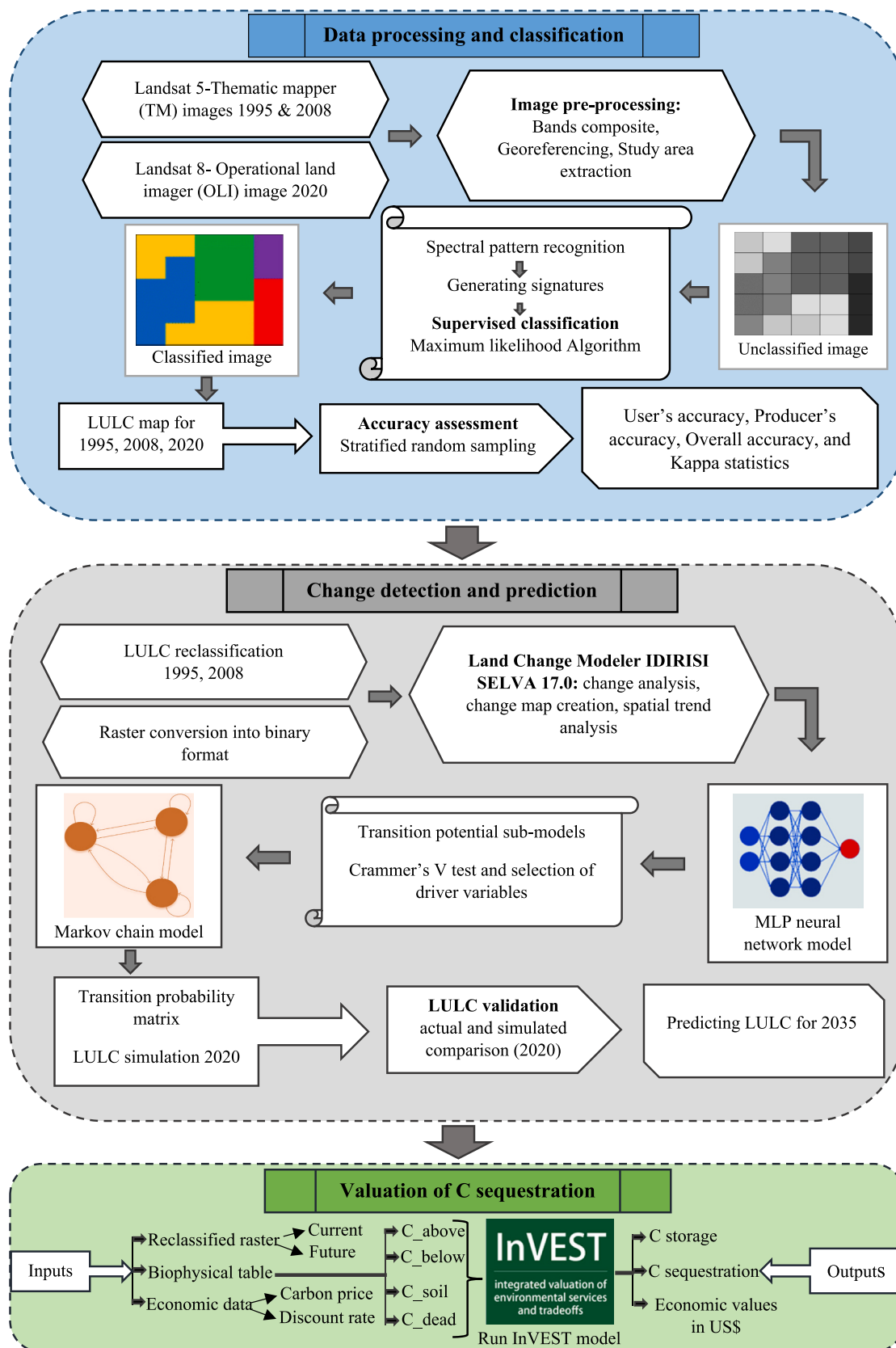


Fig. 2. Research workflow designed in three stages.

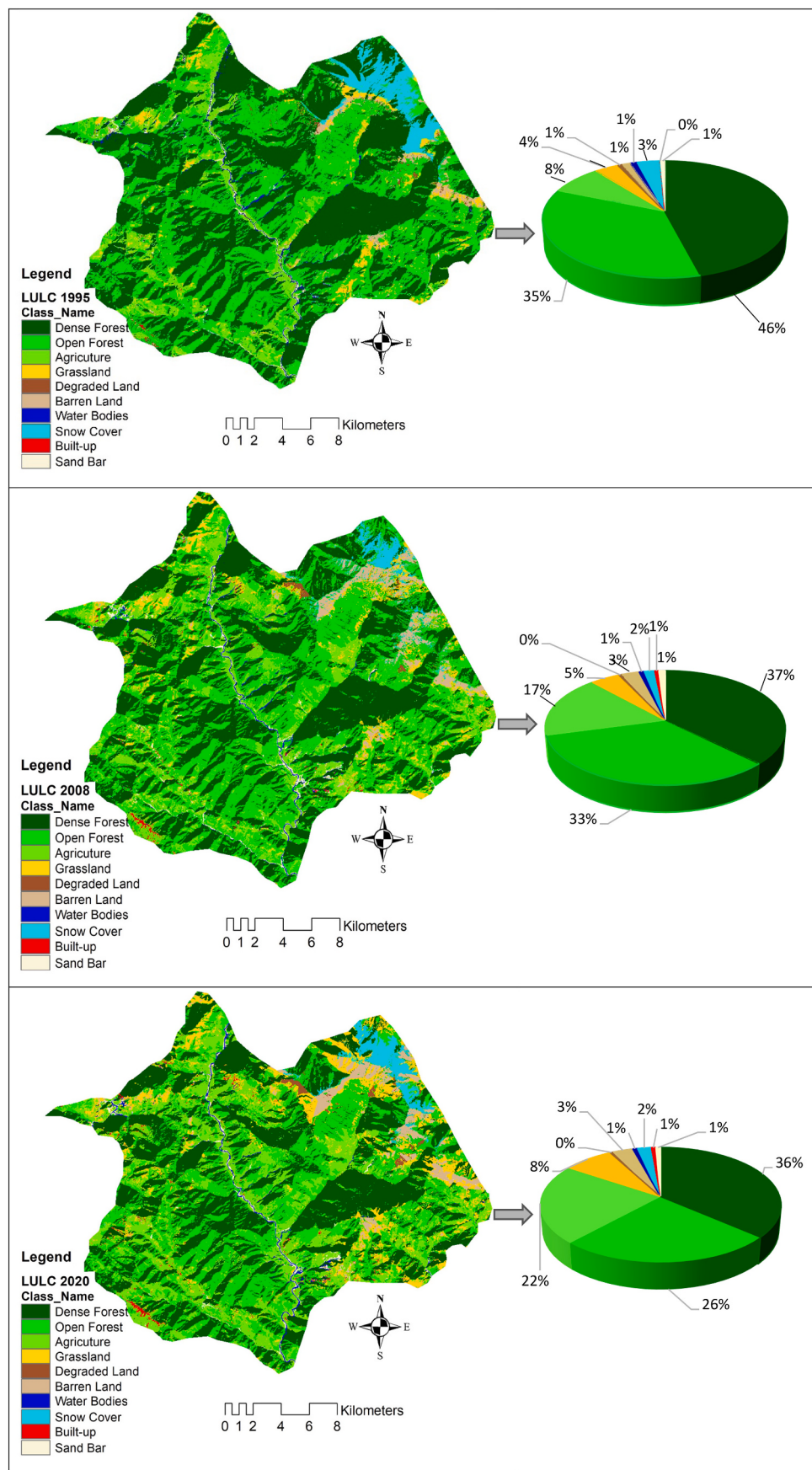


Fig. 3. LULC maps for the reference years 1995, 2008, and 2020 with respective percentage of area coverage.

Table 2

Accuracy assessment for LULC classification.

LULC classes	1995		2008		2020	
	PA (%)	UA (%)	PA (%)	UA (%)	PA (%)	UA (%)
Dense Forest	99.2	98.3	100	98.9	97.7	97.7
Open Forest	88.5	95.8	96.1	100	95.7	95.7
Agriculture	98.6	97.3	100	95.9	100	100
Grassland	100	90.9	93.3	93.3	97.4	97.4
Degraded Land	75.0	100	100	100	83.3	100
Barren Land	90.9	90.9	100	100	100	83.3
Water Bodies	100	100	66.7	100	100	100
Snow Cover	100	100	100	80.0	100	100
Built-up	100	100	100	100	100	100
Sand Bar	100	100	100	100	100	100
Overall accuracy	97.27%		98.05%		97.66%	
Overall kappa statistics (KIA)	0.96		0.97		0.97	

PA = producer's accuracy; UA = user's accuracy.

sequestration. The following inputs are required to simulate the map with the economic value (in currency/pixel) of the C sequestered:

- LULC raster maps (current and future)
- Social cost of carbon (SCC) set as a carbon price
- Market discount rate
- Annual rate of change in C price

NPV provides a current estimate of future benefits by incorporating time element as a discount rate, making it a more practical method of valuation. The discount rate is an indicator of the interests of future generations, ensuring or estimating future profits or losses (Yu et al., 2020). Within a certain range, an increase in the discount rate results in a decrease in NPV, and vice versa (Rajbanshi and Das, 2021). NPV can be calculated for C sequestration over time using the following formula for the given land parcel k (Abd El-Hamid and Hafiz, 2022; Adelisardou et al., 2022):

$$NPV_{\text{sequestration}_k} = V \frac{s_k}{y^{fut} - y^{cur}} \sum_{t=0}^{y^{fut} - y^{cur} - 1} \left(1 + \frac{i}{100}\right)^{-t} \left(1 + \frac{c}{100}\right)^{-t} \quad (7)$$

where: V = the monetary value per unit of C; s_k = the sequestered carbon in land parcel k ; y^{fut} = future year; y^{cur} = current year; i = the discount rate; and c = the annual rate of change in C price.

This study performs a sensitivity analysis across four scenarios to address existing uncertainties and evaluate the variation in NPV with respect to different carbon prices and discount rates in order to identify the most suitable scenario for C sequestration with optimal economic benefits. The established scenarios to run the analysis are described below:

- I. US\$ 86 (49–157) per t CO₂: Country-level SCC estimated for India by (Ricke et al., 2018).
- II. US\$ 25 per t CO₂: International carbon price floor (ICPF) proposed by IMF (Moritz and Gawel, 2021) in 2021 for low-income countries-LICs (in 2018 dollars) to achieve the target of Paris agreement by keeping less burden on developing countries to incentivise their participation.
- III. 3% discount rate: low societal preference for immediate benefits over future benefits.
- IV. 7% discount rate: high societal preference for immediate benefits over future benefits.

In this assessment, the annual rate of change in C price is supposed to be 0, and adopted SCC includes all the societal aspects concerned with the detrimental influence of climate change.

3. Data analysis and results

3.1. LULC change detection analysis

This section of the study delineates LULC changes from 1995 to 2035. Table 4 demonstrates the total area covered by each class (in ha) along with the percentage of area in each class and changes (gain/loss) in landcover that occurred over time. Table 4 reveals that in 1995, almost half of the area (45.88%) in AWLS was occupied by dense forest, followed by open forest (35.29%), agriculture (8.03%), grassland (3.65%), and others. In 2008, the percentage area of dense forest has drastically reduced by –4122.3 ha. In contrast, the area under agriculture has increased by 4540.5 ha. The change from 2008 to 2020 indicates that a very swift reduction in dense forest has slowed down; however, the area of open forest has decreased by –3835.2 ha. Apart from this, the area under agriculture, grassland, degraded land, barren land, snow cover, and built-up has increased. LULC change between 2020 and 2035 shows that open forest has experienced a significant loss of –3597.3 ha, while areas under agriculture and grassland have increased by 2132.28 ha and 1334.25 ha, respectively. Degraded land, built-up, and sand bar have also witnessed an increase in landcover during 2020–2035. The gain/loss visualisation for (1995–2008), (2008–2020), and (2020–2035) is depicted in Fig. 4 (in percentage).

To understand the changing pattern of land cover for the periods 1995–2020 and 2020–2035, change matrices (Table 5 and Table 6) have been obtained through area-wise cross-tabulation of LULC classes. These changes can also be examined through the graphical representation of change matrices. Fig. 5a depicts land conversion from 1995 to 2020, and Fig. 5b indicates LULC changes from 2020 to 2035. The dynamics from 1995 to 2020 show a major conversion of dense forest and open forest into agriculture by 1043.89 ha and 6131.62 ha, respectively. From 2020 to 2035, agriculture has again been subject to an increase in landcover due to the conversion of open forest into agriculture, accounting for 1479.85 ha, followed by grassland (807.28 ha). A total of 3490.49 ha of agriculture and 1270.47 ha of grassland have changed into open forest;

Table 3

Biophysical table (Mg/ha) used as input in InVEST model.

Lucode	LULC_name	C_above	C_below	C_soil	C_dead	Sources
0	Unclassified	0	0	0	0	–
1	Dense Forest	140	70	35	12	(Natural Capital Project, 2022; Piyathilake et al., 2022)
2	Open Forest	65	40	25	6	(Natural Capital Project, 2022; Rajbanshi and Das, 2021)
3	Agriculture	23	35	21	5	(Rajbanshi and Das, 2021)
4	Grassland	15	35	30	4	(Natural Capital Project, 2022; Piyathilake et al., 2022)
5	Degraded Land	0	0	0	0	–
6	Barren Land	0.1	1.9	0.8	0	(Adelisardou et al., 2022)
7	Water Bodies	2	1	10	0	(Hoque et al., 2021)
8	Snow Cover	0	0	0	0	–
9	Built-up	2	1	6.22	0	(Babbar et al., 2021; Rajbanshi and Das, 2021)
10	Sand Bar	0	0	0	0	–

Table 4

LULC statistics of 1995, 2008, 2020 and 2035 (in ha).

Class_name	Area_1995	Area_2008	Area_2020	Area_2035	Area Δ		
					(1995–2008)	(2008–2020)	(2020–2035)
Dense Forest	22,162.95 (45.88%)	18,040.68 (37.35%)	17,532.8 (36.29%)	17,036.73 (35.27%)	-4122.3	-507.87	-496.08
Open Forest	17,048.61 (35.29%)	16,181.91 (33.5%)	12,346.7 (25.55%)	8749.44 (18.11%)	-866.7	-3835.2	-3597.3
Agriculture	3879.45 (8.03%)	8419.95 (17.43%)	10,875 (22.51%)	13,007.25 (26.93%)	4540.5	2455.02	2132.28
Grassland	1765.89 (3.65%)	2207.61 (4.57%)	3750.66 (7.76%)	5084.91 (10.53%)	441.72	1543.05	1334.25
Degraded Land	342.45 (0.71%)	227.97 (0.47%)	245.34 (0.51%)	786.69 (1.63%)	-114.48	17.37	541.35
Barren Land	594.36 (1.23%)	1302.66 (2.7%)	1492.2 (3.09%)	1241.19 (2.57%)	708.3	189.54	-251.01
Water Bodies	511.11 (1.06%)	385.11 (0.8%)	357.39 (0.74%)	351.09 (0.73%)	-126	-27.72	-6.3
Snow Cover	1632.06 (3.38%)	763.29 (1.58%)	1023.93 (2.12%)	737.91 (1.53%)	-868.77	260.64	-286.02
Built-up	46.89 (0.1%)	297.54 (0.61%)	335.61 (0.69%)	609.12 (1.26%)	250.65	38.07	273.51
Sand Bar	323.46 (0.67%)	480.51 (0.99%)	347.58 (0.72%)	702.9 (1.45%)	157.05	-132.93	355.32

**Fig. 4.** Percentage of gain/loss dynamics in LULC area for (1995–2008), (2008–2020), and (2020–2035).

however, the net area under open forest in 2035 has reduced and shrank to only 18% of the total sanctuary area. Throughout the duration, agriculture has experienced a significant expansion in the area.

3.2. Transition potential mapping and Markov transition probability matrix

3.2.1. Modelling transition potential linked deriver variables using MLP algorithm

This section deals with the assessment of land use transitions and their correlation with the driver variables that have been modelled through the MLP algorithm. Before starting the calibration process

Table 5
Change matrix (1995–2020) in ha.

LULC Classes	Dense Forest	Open Forest	Agriculture	Grassland	Degraded Land	Barren Land	Water Bodies	Snow Cover	Built-up	Sand Bar
Dense Forest	16,657.92	2780.06	1043.89	992.79	37.28	114.71	137.04	251.95	88.8	57.75
Open Forest	684.17	8437.31	6131.62	1311.62	122.74	165.63	12.48	62.93	149.16	56.04
Agriculture	68.31	659.66	2811.38	204.45	4.39	38.36	26.68	4.69	34.41	72.79
Grassland	17.69	107.37	589.83	622.86	26.38	303.57	0.01	2.33	3.03	11.1
Degraded Land	1.31	32.24	88.47	100.85	27.28	45.48	2.03	3.97	5.25	8.85
Barren Land	0.48	55.44	47.61	142.81	3.79	333.53	0.01	1.07	0.19	8.04
Water Bodies	84.01	52.15	120.66	44.46	2.45	1.95	121.07	0.25	9.34	45.3
Snow Cover	38.72	177.65	0.08	225.47	10.74	479.84	0	699.87	0.78	0.9
Built-up	1.91	3.36	13.17	6.18	1.3	0.45	0.76	0.03	14.23	1.16
Sand Bar	17.62	22.42	81.26	40.26	4.2	4.88	52.54	1.28	8.59	73.22

Table 6
Change matrix (2020–2035) in ha.

LULC Classes	Dense Forest	Open Forest	Agriculture	Grassland	Degraded Land	Barren Land	Water Bodies	Snow Cover	Built-up	Sand Bar
Dense Forest	15,597.62	802.39	225.2	301.32	5.24	5.49	68.81	67.03	27.98	8.85
Open Forest	444.6	6432.52	1479.85	243.39	3.97	18.46	2.28	86.46	55.02	7.71
Agriculture	950.67	3490.49	7775.75	487.77	8.19	48.32	51.11	4.86	93.85	90.86
Grassland	369.05	1270.47	807.28	1927.19	62.03	216.03	5.16	335.46	35.49	24.16
Degraded Land	30.18	78.44	28.11	208.45	138.53	272.92	0.25	5.44	8.69	2.3
Barren Land	8.01	64.51	36.03	235.35	4.83	846.52	0.57	37.96	2.53	4.64
Water Bodies	72.55	20.89	35.18	25.25	1.41	0.79	135.37	0.82	3.32	45.51
Snow Cover	11.19	37.29	3.04	100.37	3.77	71.13	0	488.44	0.4	0.78
Built-up	56.9	84.76	218.35	111.54	7.24	3.63	15.2	0.68	78.91	12.61
Sand Bar	32.12	46.8	319.82	51.37	5.4	5.07	73.84	1.19	7.65	137.74

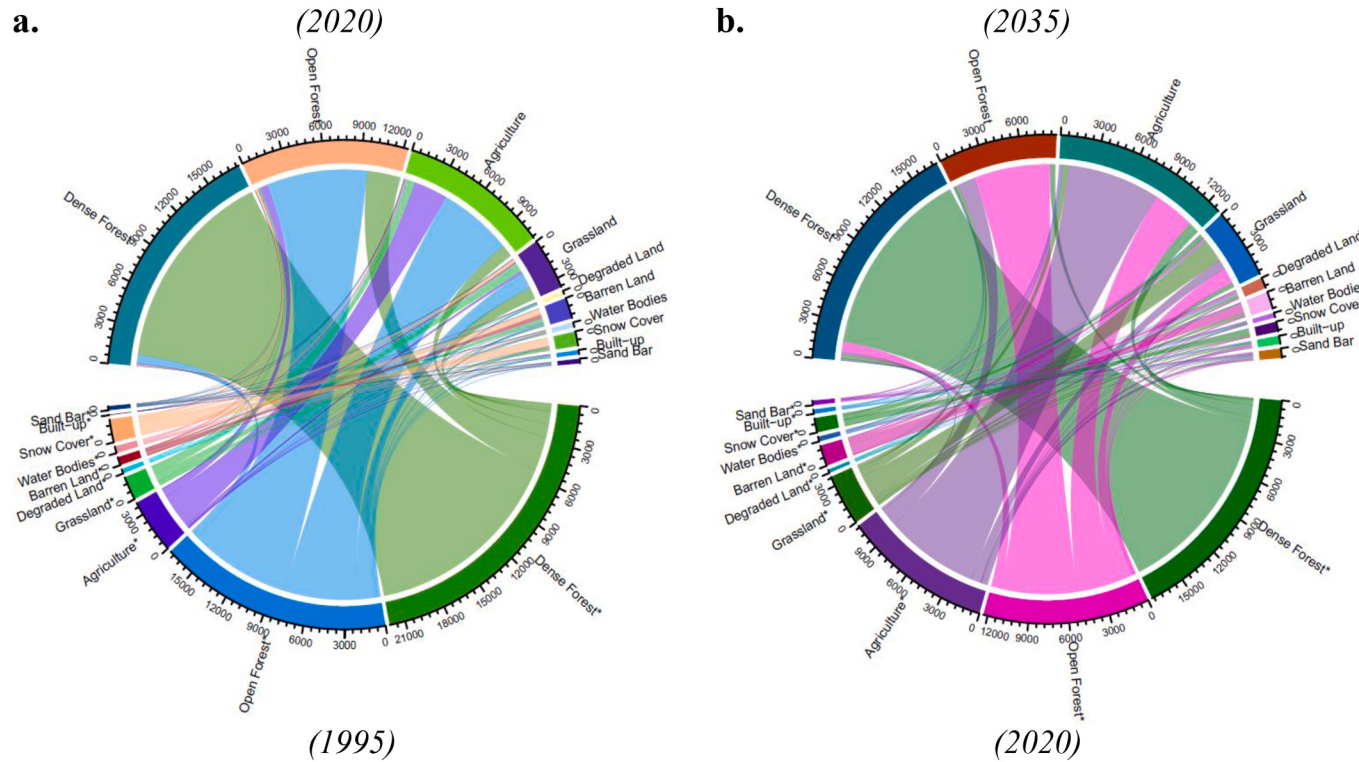


Fig. 5. Change matrix visualisation a. (1995–2020) and b. (2020–2035) area in ha.

within MLP, a few transition sub-models were developed based on major land use changes indicated by various previous studies. (Abd El-Hamid and Hafiz, 2022; Rajbanshi and Das, 2021). Five transition sub-models were taken into consideration, namely, (i) from Dense Forest to Agriculture, (ii) from Dense Forest to Degraded Land, (iii) from Open Forest to Agriculture, (iv) from Open Forest to Degraded Land, (v) Open Forest to Built-up. The driver variables are the spatial forces contributing to the

LULC transformation (Rajbanshi and Das, 2021). In this study, seven biophysical and socio-economic explanatory factors such as (a) Elevation, (b) Slope, (c) Distance from roads, (d) Distance from places, (e) Distance from buildings, (f) Distance from waterways, and (g) Distance from land use (Fig. 6) were included in the model because they play crucial roles in developing the transition potential map for LULC change dynamics. These independent variables were tested by Cramer's

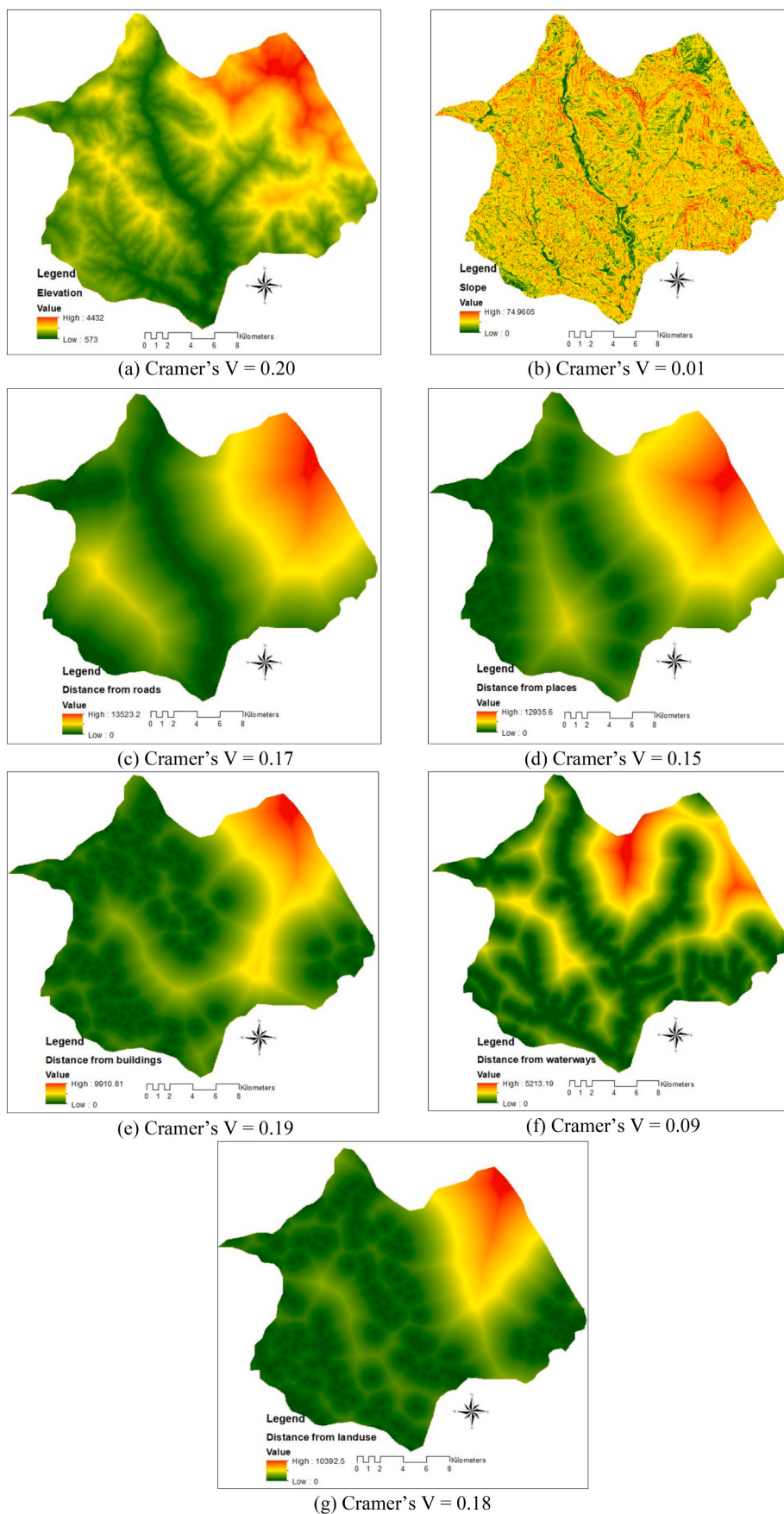


Fig. 6. Selected driver variables used for the prediction of LULC 2035.

coefficient of correlation value (Fig. 6) that varies from 0 to 1. If a variable's Cramer's V value is ≥ 0.15 , then it will be regarded as potentially useful, whereas value ≤ 0.15 will be considered less impactful for mapping the transition (Nasiri et al., 2019; Rajbanshi and Das, 2021). Cramer's V value can be calculated by the following equation (Mirici et al., 2017):

$$V = \sqrt{\frac{x^2}{N(m-1)}} \quad (8)$$

where: x^2 = Chi-square; N = Population; and m = no. of columns.

The results of Cramer's V were used as the weighting value of the driver variables while training and creating a multi-variate function in MLP modelling to predict the potential LULC transition. Fig. A.1 demonstrates the potential transition map of major land use classes between 2020 and 2035. The MLP was trained with 50% of the data, while the remaining 50% was reserved for the testing process. The MLP model parameters and performance rate are illustrated in Table 7, where skill measure and accuracy rate were observed as 0.87 and 88.79%, respectively, while keeping two stopping criteria during calibration: RMS = 0.01 and iterations = 10,000. The skill measure is represented by the following expression (Kumar and Agrawal, 2023):

$$S = \frac{[A - E(A)]}{[1 - E(A)]} \quad (9)$$

where: $E(A)$ = expected accuracy; and A = measured accuracy.

The expected accuracy $E(A)$ can be computed using the following expression (Kumar and Agrawal, 2023):

$$E(A) = \frac{1}{T + P} \quad (10)$$

where: T = no. of transition in the sub-models; and P = persistence class in the sub-models.

3.2.2. Markov transition probability matrix

The Markov chain model has the capacity to capture the LULC transition by assessing the gains and losses, persistence, and specific conversions in landscapes utilising quantitative data information and maps (Beroho et al., 2023). The quantity of transformation in the feature class for one-period interval is represented by the transition probability matrix, which is a square matrix (10×10) where the value of probability ranges between 0 and 1; 0 means no transition is possible, and 1 means a transition is certainly happening (Kumar and Agrawal, 2023; Marko et al., 2016). The columns of the matrix indicate new LULC classes (in the year 2035), whereas the rows denote the previous LULC classes (in the year 2020). The diagonal of the matrix signifies the possibility of persistence in the LULC categories, while the non-diagonal elements in the matrix demonstrate the likelihood of transition between

Table 7
MLP parameters and performance.

S/N	Variables	Results
1.	Input layer neurons	8
2.	Hidden layer nodes	10
3.	Output layer neurons	8
4.	Requested samples per class	1688
5.	Start learning rate	0.0008
6.	End learning rate	0.0001
7.	Momentum factor	0.5
8.	Sigmoid constant	1.0
9.	Iterations	10,000
10.	Acceptable RMS	0.01
11.	Training RMS	0.1430
12.	Testing RMS	0.1446
13.	Accuracy Rate	88.79%
14	Skill measure (%)	0.8719

two time periods, that is, 2020–2035 in this study (Table 8). Except for water bodies, snow cover, built-up, and sand bar, all the other classes have persistence possibility $>50\%$, and especially dense forest has the highest chance (nearly 90%) to remain in the same class since AWLS is a protected area, so less conversion is possible. Fig. 7 depicts the graphical view of the transition matrix indicating agriculture, open forest, and grassland to be more dynamic classes as the conversions in these classes are appearing more, such as open forest to agriculture (28%), grassland to agriculture (13%), degraded land to grassland (26%), etc.

3.3. Future prediction with land change modeler (LCM) and validation

LULC scenarios were simulated incorporating MLPnn-MC modelling based on change analysis and transition potential within the LCM module. Validation of simulated LULC map is an integral part of geo-spatial modelling for examining the functionality, acceptance, and reliability of the prediction. Cohen's kappa index (K-index) is a broadly accepted statistic to measure the extent of congruence, including the goodness-of-fit between actual and simulated maps for the identical year that is correlated for correctness by chance (Khawaldah et al., 2020; Nath et al., 2020). Kappa-index value varies from +1 to -1, where a positive value indicates improved agreement and a negative value infers insufficient agreement. K-index technique renders pixel-by-pixel calculations to seek the precision of simulation (Omar et al., 2014). The value range of K-indices, strength of agreement, and % of reliability are depicted in Table A.1. Kappa-indices (K_{no} , $K_{location}$, $K_{locationStrata}$, $K_{standard}$) and agreement/disagreement constituents for the simulated map of 2020 are compiled from the validation module within IDRISI Selva software (Table 9). The blend of K-indices offers substantial investigation of overall accuracy subject to both location and quantity (Leta et al., 2021). K_{no} (no information), $K_{location}$ (grid-cell network location), $K_{locationStrata}$ (stratum-level location), and $K_{standard}$ (standard kappa) can be formalised as follows; Eqs. (11–14) (Omar et al., 2014; Singh et al., 2015):

$$K_{no} = \frac{M_m N_n}{P_p - N_n} \quad (11)$$

$$K_{location} = \frac{M_m N_m}{P_m - N_m} \quad (12)$$

$$K_{locationStratum} = \frac{M_m H_m}{K_m - H_m} \quad (13)$$

$$K_{standard} = \frac{M_m N_n}{P_p - N_m} \quad (14)$$

where: N_n = no information; H_m = medium stratum level information; M_m, N_m = medium grid cell level information; K_m = perfect grid cell level information; and P_p = perfect grid cell level information all over the map.

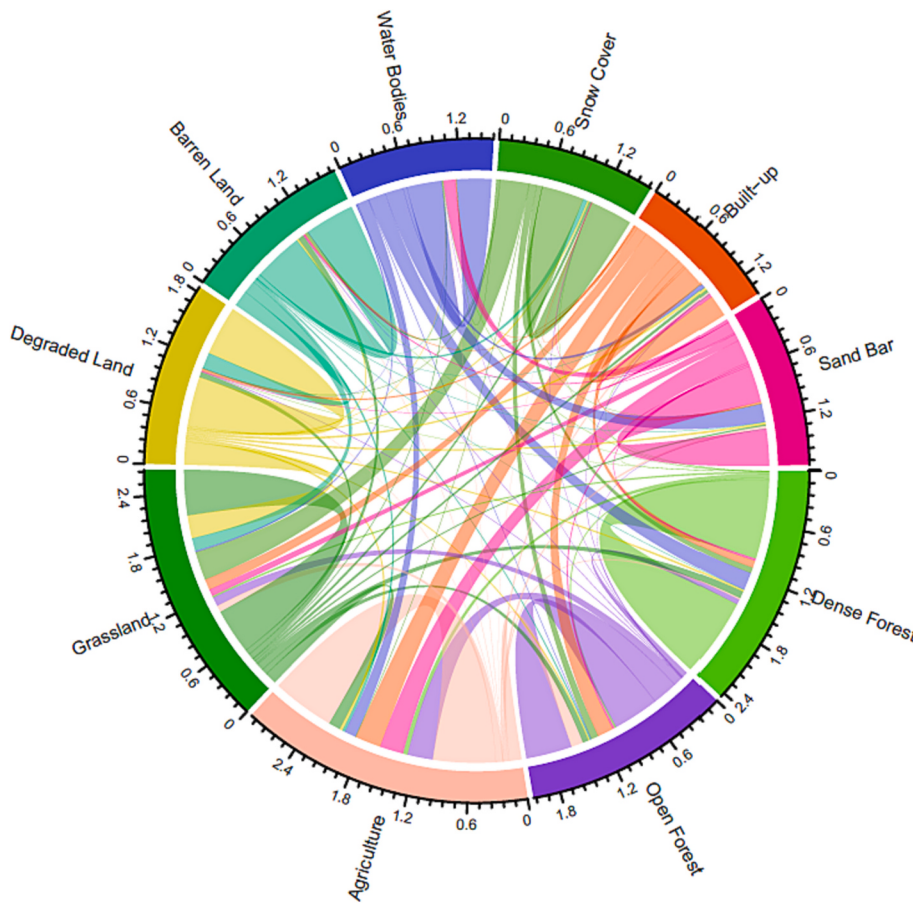
Table 9 furnishes the statistical values of K-indices calculated for the reference (2020) and simulated (2020) LULC maps, which indicate the performance of the projection. Many studies (Mirici et al., 2017; Nath et al., 2020) have stated that acceptable accuracy of the predictive model must be ≥ 0.70 for LULC modelling. In this study, from Table 9, K-indices of agreement: $K_{no} = 0.75$, $K_{location} = 0.70$, $K_{locationStratum} = 0.70$, and $K_{standard} = 0.68$ have the average value >0.70 , indicating that the actual and projected LULC are $>70\%$ identical. Agreement/disagreement values are presented in Table 9. The disagreement value between two maps is often low because of quantity errors (0.0242) and not due to allocation errors (0.2158). The agreement parameters show an overall good score (76%) of agreement. The results designate a higher ability of model to project future LULC trajectory, mainly in location rather than quantity, which means the model has good potential for future simulation with the specification in location.

Further in the study, the Figure of Merit (FOM) method (embedded

Table 8

Transition matrix (2020–2035).

LULC Classes	Dense Forest	Open Forest	Agriculture	Grassland	Degraded Land	Barren Land	Water Bodies	Snow Cover	Built-up	Sand Bar
Dense Forest	0.891	0.022	0.053	0.020	0.002	0.001	0.004	0.001	0.003	0.002
Open Forest	0.058	0.522	0.287	0.102	0.006	0.005	0.002	0.003	0.007	0.004
Agriculture	0.018	0.135	0.709	0.076	0.002	0.003	0.003	0	0.020	0.029
Grassland	0.080	0.066	0.132	0.515	0.057	0.063	0.007	0.029	0.031	0.015
Degraded Land	0.022	0.016	0.034	0.260	0.561	0.022	0.005	0.018	0.032	0.025
Barren Land	0.003	0.013	0.032	0.145	0.182	0.565	0.001	0.050	0.003	0.004
Water Bodies	0.199	0.005	0.129	0.015	0.000	0.002	0.396	0	0.045	0.205
Snow Cover	0.064	0.083	0.005	0.324	0.005	0.035	0.001	0.477	0.001	0.001
Built-up	0.080	0.182	0.293	0.122	0.027	0.008	0.010	0.002	0.248	0.025
Sand Bar	0.024	0.022	0.266	0.078	0.005	0.016	0.132	0.002	0.036	0.415

**Fig. 7.** Graphical representation of transition matrix (2020–2035).**Table 9**

Validation results derived from the validation module in IDRISI Selva 17.0.

k-Index of agreement	Value
K _{no}	0.75
K _{location}	0.70
K _{locationStrata}	0.70
K _{standard}	0.68
<i>Agreement/Disagreement constituents</i>	
AgreementChance	0.0909
AgreementQuantity	0.1744
AgreementStrata	0.0000
AgreementGridcell	0.4947
DisagreeGridcell	0.2158
DisagreeStrata	0.0000
DisagreeQuantity	0.0242

in the LCM module) is applied to test the predictive ability of the model using the following formula (Eq. (15)) (Kumar et al., 2023), which generally acts as a supplement to K-indices in assessing the accuracy of LULC simulation (Zhang et al., 2023).

$$FOM = \frac{\text{Hits}}{\text{Hits} + \text{False Alarms} + \text{Misses}} * 100 \quad (15)$$

FOM is a three-map comparison technique (2008 reference map, 2020 reference map, and 2020 simulated map) used to evaluate the persistence of grid-cells between the reference and simulated maps, which ranges from 0 (no overlapping) to 100% (perfect overlapping) between actual and projected maps (Pontius et al., 2008). The result of FOM application is a map, visualising the four components, viz., Hits (projected change that persisted in reality), False Alarms (predicted change that did not occur in reality), Misses (predicted changes that stayed unchanged), and Null Success (no change prediction occurred) (Fig. A.2). The calculated FOM is 9.60%, an acceptable value for robust

predictive ability (Kumar et al., 2023), which is more than (8.30%, 8.76%) as achieved by the previous studies (Kou et al., 2023; Kumar et al., 2023) and close to 10.4%, as achieved by Camacho Olmedo et al. (2013). The projected LULC maps for 2020 and 2035 are presented in Fig. 8.

As a cross-validation of the model, chi-square test was applied to estimate if the actual (O) and predicted (E) LULC maps for 2020 match each other or not (Table 10). The formulated hypothesis is expressed below:

H_0 : There is no significant difference between actual and simulated LULC for 2020.

H_1 : There is significant difference between actual and simulated LULC for 2020.

The rejection level was fixed at $\alpha = 0.05$ with $df = 9$, where the computed value of X^2 (2.767) < critical value of X^2 (16.919). Hence, the null hypothesis is accepted, indicating no difference between the simulated and reference maps of 2020.

3.4. Mapping of carbon storage and sequestration (CS & S)

The LULC class-wise distribution of CS values in AWLS from 1995 to 2035 is illustrated in Fig. 9, in which the 'size of the bar' has reduced by 2035, indicating the loss of C content in the whole study area in future due to increasing human-wildlife conflicts and rapid eradication of healthy and long-living biomass in the area. Among all the land use classes, dense forest has the highest C-density, followed by open forest, agriculture, and grassland; however, over time, C content has decreased in dense forest (from 1995: 5695878.41 Mg/ha to 2035: 4378439.81 Mg/ha) and open forest (from 1995: 2318610.92 Mg/ha to 2035: 1189923.82 Mg/ha) whereas C-density in agriculture and grassland has increased by 2035 because of the conversion of forested area into other classes such as agriculture, grassland, and others (as demonstrated in the change matrices: Tables 5 and 6).

Furthermore, the calculation of net change in C or estimation of C sequestration is also performed in the InVEST model using current and future LULC maps, assuming that any change that occurred in CS was due to the conversion of one land into another. The model has also produced raster maps showing CS & S in each grid-cell (in Mg/pixel) for the entire study area. Hence, any pixel that does not alter its LULC

Table 10
Validation of LULC prediction by Chi-Square test.

Class name	Actual 2020 (O)	Predict 2020 (E)	(O-E)	(O-E) ²	(O-E) ² / E
Dense Forest	175.33	176.87	1.54	2.371	0.013
Open Forest	123.47	120.24	-3.22	10.368	0.086
Agriculture	108.75	115.74	6.99	48.860	0.422
Grassland	37.50	31.38	-6.12	37.454	1.193
Degraded Land	2.45	2.88	0.43	0.184	0.063
Barren Land	14.92	12.70	-2.22	4.928	0.388
Water Bodies	3.57	3.19	-0.37	0.137	0.042
Snow Cover	10.24	11.30	1.06	1.123	0.099
Built-up	3.35	3.89	0.54	0.291	0.074
Sand Bar	3.47	4.85	1.37	1.877	0.387

Note: Chi square (X^2) = $\sum(O-E)^2/E = 2.767$, Degree of Freedom (df) = 9, p-value = 0.972, and Significance level (α) = 0.05, Critical value (X^2) = 16.919; Columns O and E are area of each LULC class in km².

classes will have no gain/loss of C sequestration over time. Due to the focus of the present study on forests, mapping of CS & S for the forested area (dense and open forests) has been done separately in the InVEST model (Fig. 10: a, b, c), and for comparative analysis, CS & S are also mapped, including all classes in the region (Fig. 10: d, e, f) for the duration 2020–2035. The difference in CS between Fig. 10a and Fig. 10b is very apparent due to the drastic loss of forest cover from 2020 to 2035, whereas the difference in total CS between Fig. 10d and Fig. 10e is comparatively less as the carbon loss due to the forest loss is compensated by the other LULC classes in the area, primarily by agriculture and grassland. Fig. 10c indicates C sequestration in forests (Mg/pixel) and Fig. 10f indicates C sequestration in all land use classes (Mg/pixel), where a positive value shows gain in C and a negative value shows loss of C into the atmosphere.

The graphical representation of CS & S in forests and mean forest C storage (Mg/ha) is given by Fig. 11a, and the graphical representation of CS & S in all classes and mean C storage across the study area is given by Fig. 11b for the time period 1995–2035. Fig. 11a shows a decreasing trend of C loss in forests, which is fast from 2008 (-1,177,294.6 Mg of C/ha) to 2020 (-652,105.71 Mg of C/ha) and quite slow from 2020 to

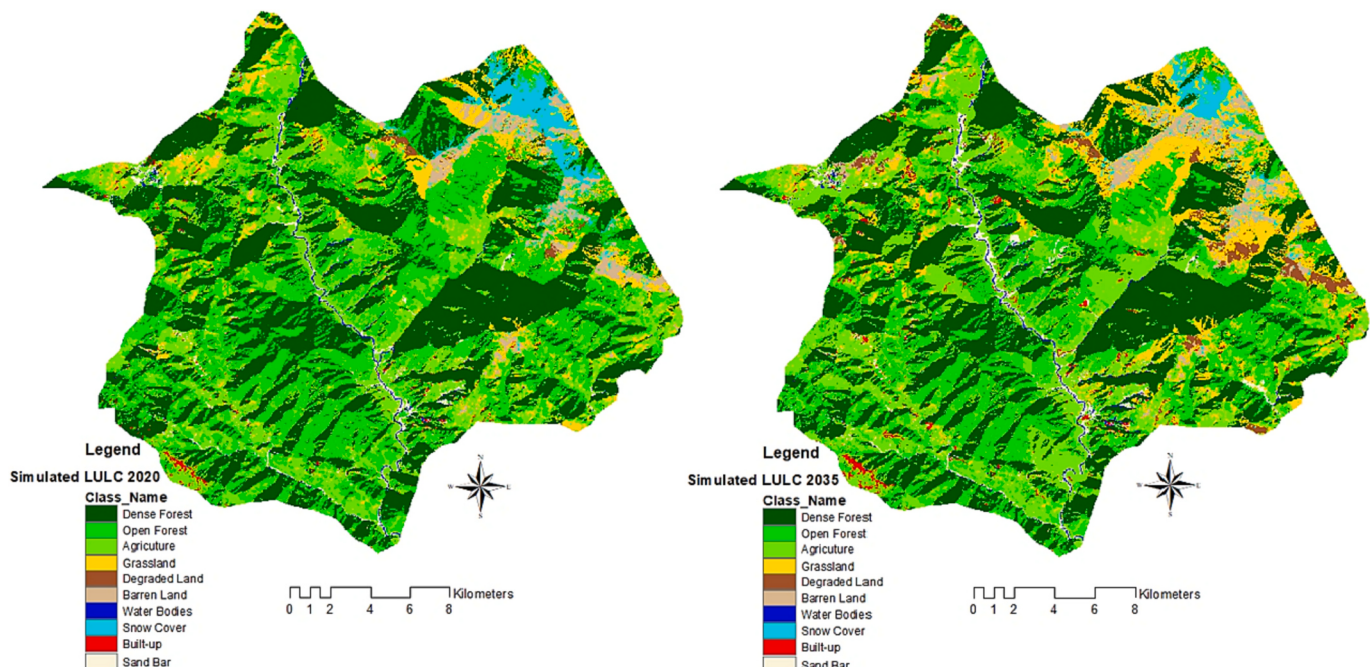


Fig. 8. Simulated LULC maps for 2020 (left) and 2035 (right).

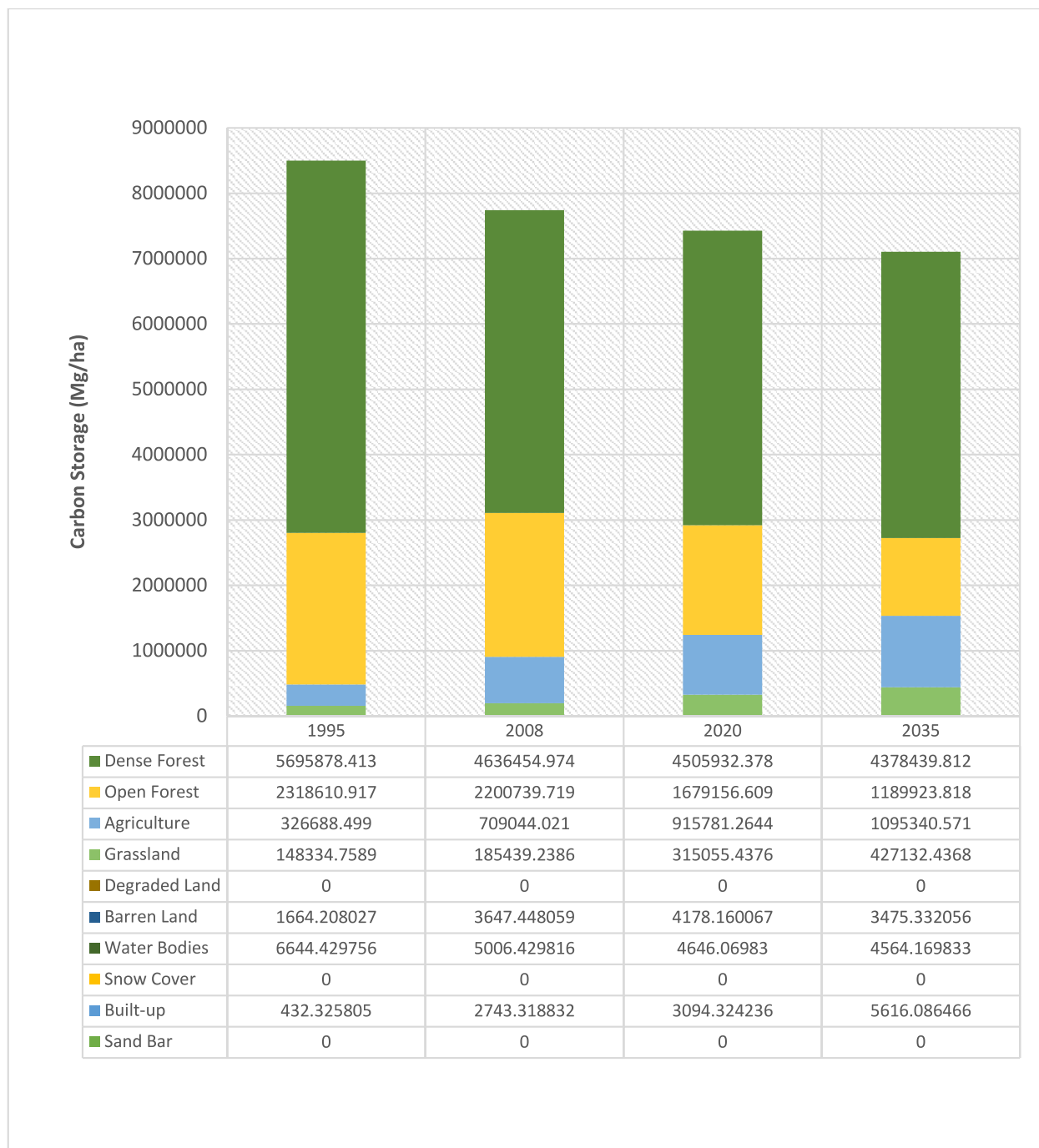


Fig. 9. Class-wise content of carbon storage (Mg/ha).

2035 ($-616,725.36$ Mg of C/ha). Although C loss has increased over time, the rate of increase is decreasing, possibly due to the declaration of the 'Eco-Sensitive Zone' (non-development zone) of the sanctuary and increased protection of forests. While in Fig. 11b, the loss of C across the study area has decreased over time, and the total loss of C is also less than that of the forested area. The mean value of C storage in forests by 2035 is also less (10.36 Mg/ha) than the mean value of C in the whole area (13.24 Mg/ha), indicating the massive destruction of forest land cover in the region.

3.5. Valuation of carbon sequestration

The economic monitoring of C sequestration in terms of NPV is

undertaken by carrying out the sensitivity analysis under four scenarios of different C prices and discount rates for the period 2020–2035. Fig. 12 demonstrates separate valuations for forests and all LULC classes in the study area, where the negative trend of NPV is indicating huge economic losses due to the increasing cost of C in the future by 2035 as a consequence of the continuous reduction in projected forest cover. A C price of US\$ 86 reflects nearly four times more loss in economic value of C sequestration (\sim US\$ -53 million) than at US\$ 25 (\sim US\$ -15 million) for both 3% and 7% discount rates. The combined valuation of all land use classes shows comparatively less economic loss as the lost carbon was offset by other classes. It is noticeable that as the discount rate decreases, the NPV for C sequestration increases. From Fig. 12, the highest economic loss was observed in forests (US\$ -52.92 million at 3% discount

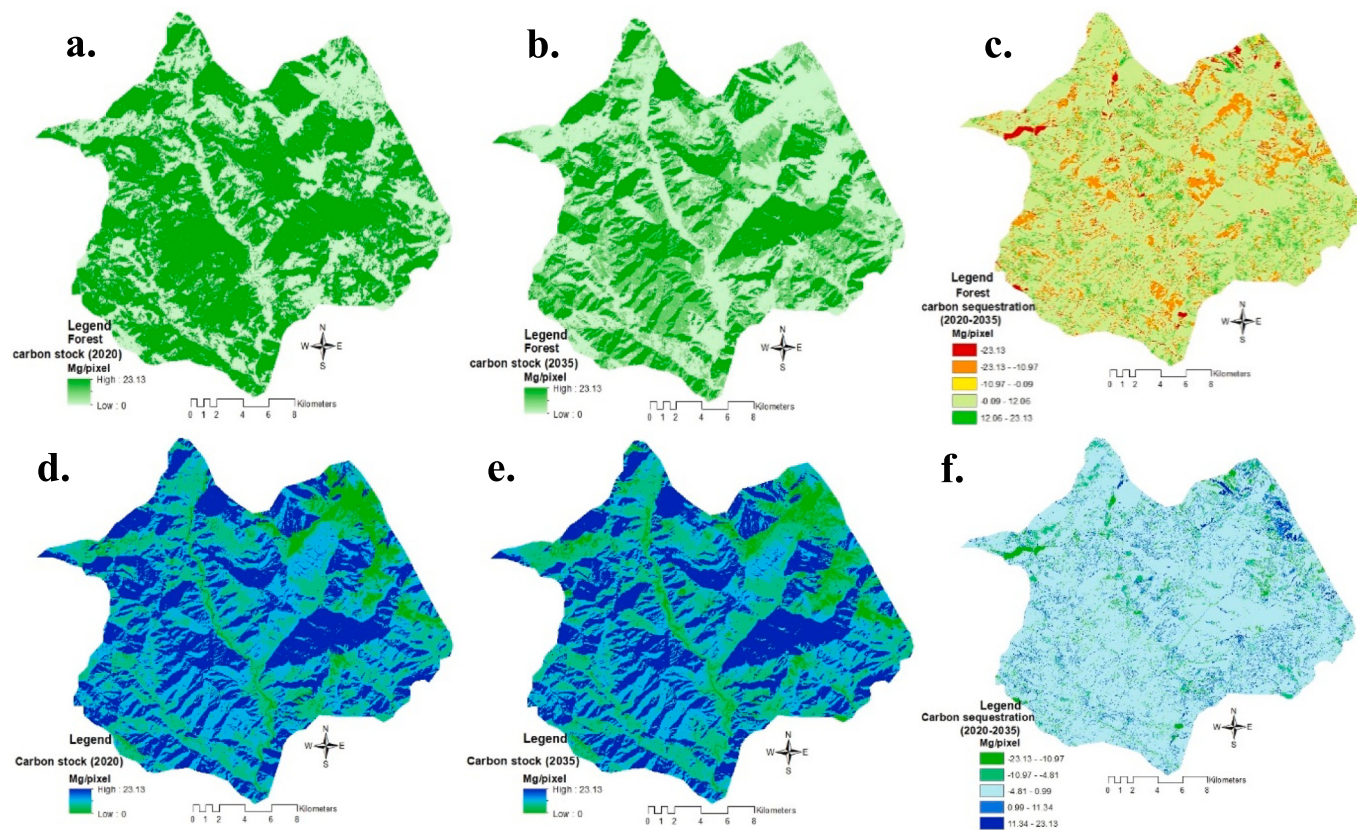


Fig. 10. (a) Forest carbon stock in 2020, (b) Forest carbon stock in 2035, (c) Forest carbon sequestration (2020–2035), (d) Carbon stock in all LULC classes in 2020, (e) Carbon stock in all LULC classes in 2035, (f) Carbon sequestration in all LULC classes (2020–2035).

rate and US\$ 86 carbon price), whereas the lowest loss was observed in the combined valuation of all classes (US\$ -8.04 million at 7% discount rate: preference to immediate benefit and US\$ 25/t CO₂ – low carbon price).

4. Discussion

The present research study deals with the dynamics of C sequestration and its economic valuation in AWLS, western Himalaya, a part of the protected area network of the IHR. Mountainous ecosystems are considered significant for environmental prosperity and economic well-being (Tewari et al., 2017); therefore, CS & S assessment is indispensable for ecosystem health monitoring and financial accounting in these landscapes. The AWLS is highly prone to anthropogenic pressures such as cutting, lopping, fire, and grazing, as well as natural adversities, including abnormal floods, landslides, and droughts (Barnett et al., 2005), causing loss to the natural structure of biodiversity and its capacity to maintain the climatic and atmospheric balance. Forests have been discovered to possess virtues that can rejuvenate and strengthen the potential of ecosystems against both natural hazards and human-caused distortions by acting as C sinks and controlling climate, regulating hydrology, recreating soil formation, etc., in terrestrial ecosystems (Singh, 2007). The cost of natural products such as foodgrains, drinking water, and hydro-electricity would be so high if environmental services and products were fully accounted for in monetary terms. However, presently, people do not pay enough for these natural facilities, and due to this, natural resources are subject to deterioration and eventually collapse, leaving the next generation with fewer options and depleted natural capital (Singh, 2007). A study by Ouyang et al. (2016) has reported China's first national ecosystem assessment (2000–2010), drafted to quantify and manage the maintenance of ecosystem services such as C sequestration, food production, soil retention, water retention,

flood control, sandstorm prevention, and protection of habitat for biological diversity. As a result, they experienced improvements in these services by investing in natural capital.

Natural resource capitalization and payment for ecosystem services are such potential exercises that can reverse the damages to the ecosystem (Kangas and Ollikainen, 2022; Kaur et al., 2022). Singh (2007) has estimated the economic value of forest ecosystem, which is ~US\$ 2.4 billion/yr for Uttarakhand, and at the IHR level, it is ~US\$ 21 billion/yr for 65 million tonnes of C/yr (forest biomass + forest soil). Tolangay and Moktan (2020) reported 3697.05 Mg of C/ha estimated for the western Himalayan region (WHR), whereas according to Dangwal et al. (2022), ecological rehabilitation in sub-tropical forests of WHR contributes to 1.36% of the annual increase in aboveground C storage. But economic valuation of C sequestration in WHR region is absent; moreover, regarding AWLS, located in WHR, there are studies which have discussed “Diversity, extraction and status of fodder species in AWLS” (Samant et al., 2006), “Forest vegetation responses to anthropogenic pressure: a case from AWLS” (Bisht et al., 2023), “Status and distribution pattern of coarse woody debris in AWLS” (Adhikari, 2009), and subjects like these, but there is no literature available on C sequestration accumulation in AWLS, nor has an economic accounting of it been found. In spite of being uniquely rich in ecosystem biodiversity and having huge potential for environmental services, AWLS has long been considered as low-profile protected area (Rawal and Dhar, 2001), which lately gained the attention of researchers mainly after the declaration of the ‘Eco-Sensitive Zone’ of the sanctuary. The present study attempts to bridge this gap by conducting the economic value approximation of C sequestration in the forests of AWLS as a special focus of the study, along with the valuation of C sequestration across the landscape for a comparative analysis.

Monetary valuation of C sequestration in NPV seeks extensive computation incorporating recent market C prices, discount rates, and

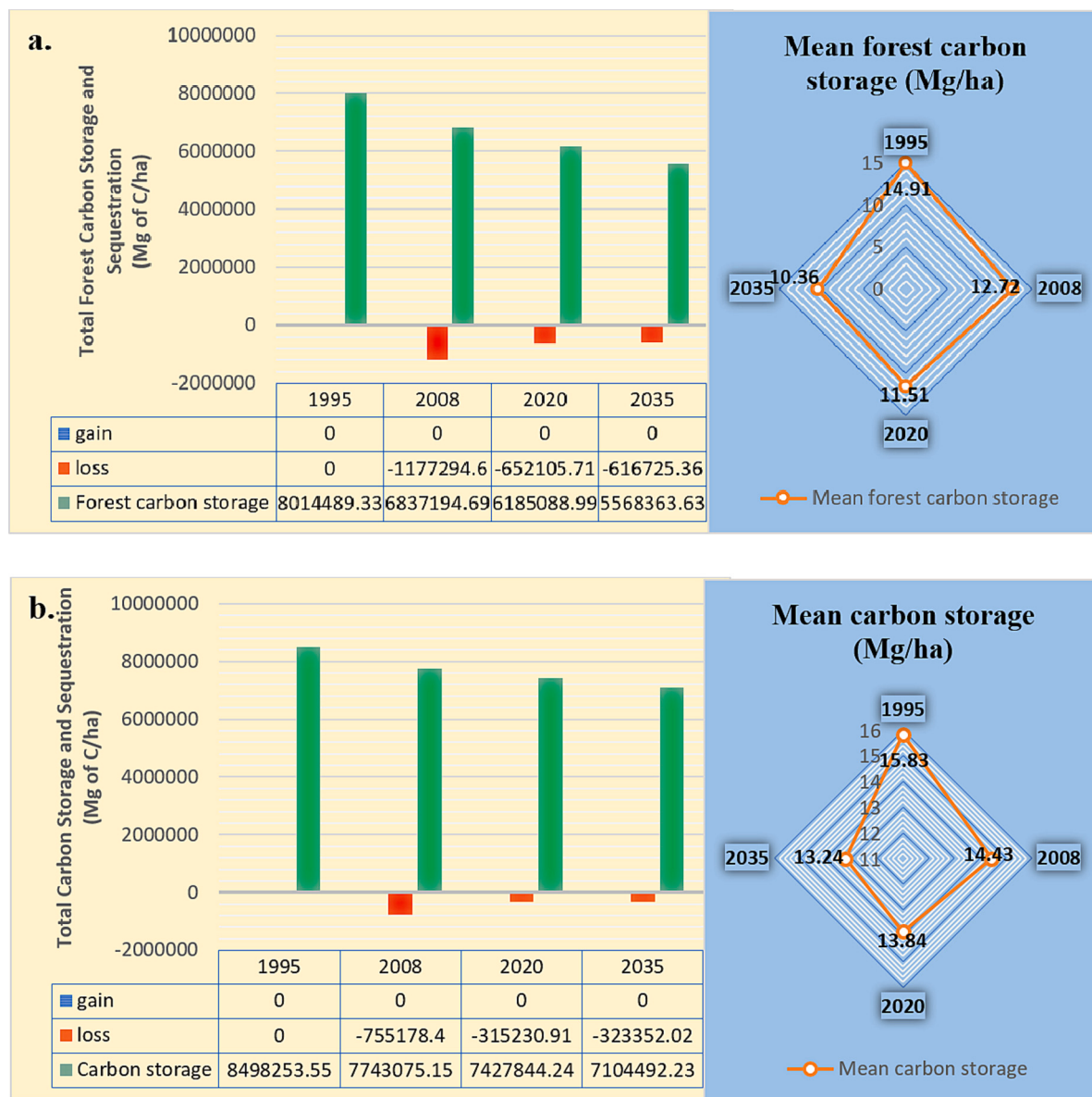


Fig. 11. Comparison of carbon storage and sequestration changes from 1995 to 2035 in forests (a) and all classes (b).

social value of C sequestration. Simulation of NPV for C sequestration was derived from the InVEST model, which also integrates LULC scenarios to minimise the complexity of assessing the spatial-temporal impact of LULC distribution on CS & S at the regional scale from 2020 to 2035. This research adopts a mix of different carbon prices and discount rates to address future risks and uncertainties and to explore the variation in NPV as a response to these scenarios. US\$ 86/t CO₂ (country-level carbon price) was applied in this study, which was estimated by Ricke et al. (2018) using current climate model projections, empirical climate-based economic damages, and socio-economic prognosis. On the other hand, US\$ 25/t CO₂ (international carbon price for LUCs) was undertaken in the study as proposed by the International Monetary Fund (IMF), considering the different stages of economic development to stimulate greater participation (Moritz and Gawel, 2021) in achieving the Paris target. India does not have any explicit C price (OECD, 2022), such initiatives will encourage countries to take part in global climate change mitigation. Furthermore, this study has tried to investigate the correlation between NPV and C sequestration, and the result reveals a high degree of positive linear association ($R^2 = 1$), signifying that with an increase in C sequestration, the economic

value of C will also rise under the given discount rate and C price (Yu et al., 2020).

Very few studies have calculated the economic value of C sequestration for forests separately from other LULC classes; however, a study conducted by (Pache et al., 2021) in Retezat National Park, Romania, reveals an economic gain of US\$ 34.12 million through FCS at US\$ 60/t CO₂ SCC, in contrast to the negative outcome of the present study, which shows an economic loss equal to about US\$ -53 million. This raises a serious concern for the protection of forests in the study region. The rapid destruction and loss of forest cover are consequences of increased extractive pressure (Bisht et al., 2023) and agriculture land expansion in the study area. Other studies (Avtar et al., 2022; Fernandes et al., 2020) have also identified agriculture as a major driver for LULC transitions. The findings of the present study for the economic value of all LULC classes synchronise with Rajbanshi and Das (2021), who have reported a similar economic loss (US\$ -8.75 million at 3% discount rate and US\$ -7.25 million at 7% discount rate) as found in the current study (US\$ -8.06 million at 3% discount rate and US\$ -8.04 million at 7% discount rate). A study conducted by Avtar et al. (2022) also reveals a similar negative trend in NPV, showing an economic loss of US\$ -1485.490

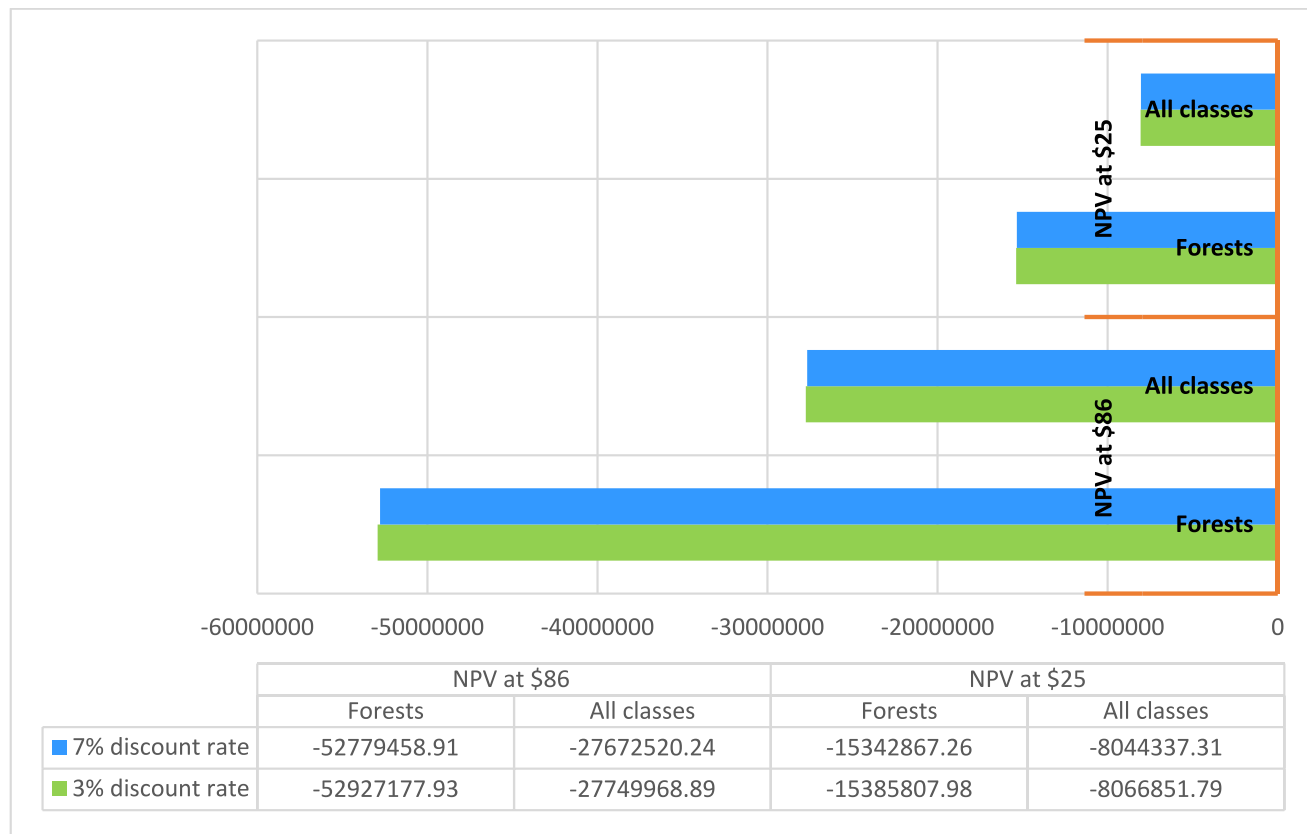


Fig. 12. Net present value (NPV) of carbon sequestration/loss in currency (US\$)/pixel (2020–2035).

million from 2020 to 2040 at US\$ 51/t CO₂ SCC and 3% discount rate. This contrasts with the economic gain of US\$ 45 million at a rate of US\$ 110/t CO₂ SCC, as reported by Adelisardou et al. (2022), achieved through the execution of environmentally sound planning. This suggests that economic gain in AWLS could be realised if intensive forest protection initiatives, such as the National Afforestation Programme (NAP), Forest Fire Prevention & Management Scheme (FFPM), and Green India Mission (GIM) are adopted. The REDD+ (Reducing Emissions from Deforestation and Forest Degradation) framework provides guidance for sustainable forest management and protection of biodiversity while upholding the rights of local residents and forest products. In addition to this, REDD+ extends financial rewards for C storage enhancement and stabilisation in forests (Verma and Kumar Ghosh, 2022). This study can be very relevant and useful in providing baseline information and necessary assistance for successfully implementing the REDD+ project. The differences between existing and current literature show uncertainty in monetary valuation and preferences of future generations for atmospheric C mitigation (Abd El-Hamid and Hafiz, 2022).

4.1. Limitations

- Maximum Likelihood Classifier is very sensitive to the distribution of LULC classes in feature space and choice of training samples, although this study yields a satisfactory range of classification accuracy.
- While deducing the projection, climatic factors, i.e., temperature and precipitation, and socio-economic elements such as population and agricultural labour force have been ignored.
- Inconsiderate selection of sub-transition models and driver variables in LCM modular can generate misleading projection.
- Due to time and financial constraints, direct measurement of C-density in each pool is avoided.

– The limitation of the InVEST model is that it presumes that C storage in each LULC class does not alter over time, which dramatically simplifies the process of the C cycle.

5. Conclusion

This study is focused on the assessment of carbon storage and sequestration (CS & S) and its economic valuation in AWLS by incorporating a fusion of remote sensing, mathematical, and machine learning algorithm-based hybrid modelling. MLPnn-MC model is used to simulate the expected shape of the study area in 2035. The InVEST model renders dynamics of C mapping over space and time, integrating economic dimensions. The main aim of the study is to investigate the spatial-temporal impact of LULC transition on CS & S capacity and associated economic gain/loss of these changes. The sensitivity analysis has been performed by establishing four scenarios with a mix of social cost of C values and societal choices as discount rates to observe the variation in NPV. Due to a huge loss of forest land cover and expansion of agriculture and grassland, the results show substantial economic losses from 2020 to 2035. Despite being a protected area, human-wildlife conflicts have been the main cause of biodiversity destruction and loss of C capture potential in the study area. Different preventive measures have been implemented by the local and national governments. Recently, the Union Environment Ministry declared the area an Eco-Sensitive Zone (ESZ) and reduced the sanctuary sprawl from 600 km² to 454.65 km² by keeping 111 villages out of the ESZ to halt biotic interference and possible unnatural anthropogenic activities.

The present study suggests identifying (i) the forest species susceptible to invasion, (ii) compositional transitions affecting the overall forest diversity, and (iii) possible responsible factors causing the generation of non-native species in the Western Himalayan territory, so that strict ecological protection measures can be taken for the sustainable utilisation and natural regeneration of rare native forest-species, which

are critical for providing security for future carbon supplies. It is also recommended to increase the plant diversity in order to revive the distortions and enhance the C stock in the sanctuary. Some high-density, fast-growing tree species or fodder and fuelwood plants are advised to be planted along the corridors of the villages to reduce the exploitation of critical natural plants by the local communities. On the other side, financial incentives are the most practical way of ensuring ecosystem conservation. Four financial scenarios have been discussed in the study; however, the most suitable scenario depends on the emission trajectories and society and government preferences regarding climate mitigation actions. Although carbon market-based practices are at an initial stage and suffering from various drawbacks, developing a potential carbon market, free from the influence of market failure, externalities, property rights, and uncertain C prices, can provide an impactful synergy for global climate change mitigation.

In forthcoming work, the identified limitations can be overcome by integrating factors such as forest composition and regeneration pattern, forest age, rain fall, and climate change, which will yield a more accurate simulation for better carbon mapping and the successful implication

of carbon trading markets.

CRediT authorship contribution statement

Pragati Verma: Writing – original draft, Visualization, Formal analysis, Conceptualization. **Azizur Rahman Siddiqui:** Supervision, Methodology. **Nitesh Kumar Mourya:** Software, Data curation. **Ahanthem Rebika Devi:** Writing – review & editing, Resources.

Declaration of Competing Interest

The authors declare that they have no known competing financial interests or personal relationships that could have appeared to influence the work reported in this paper.

Data availability

Data will be made available on request.

Appendix A. Appendix

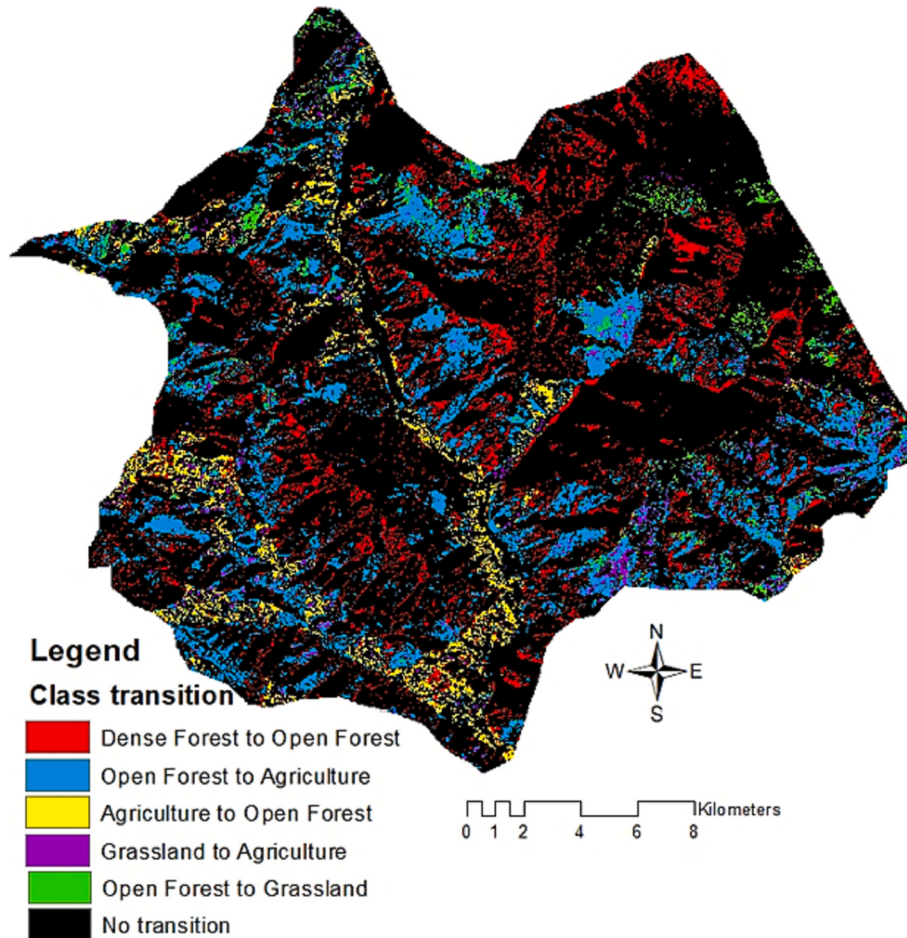


Fig. A.1. LULC Class transition map (2020–2035).

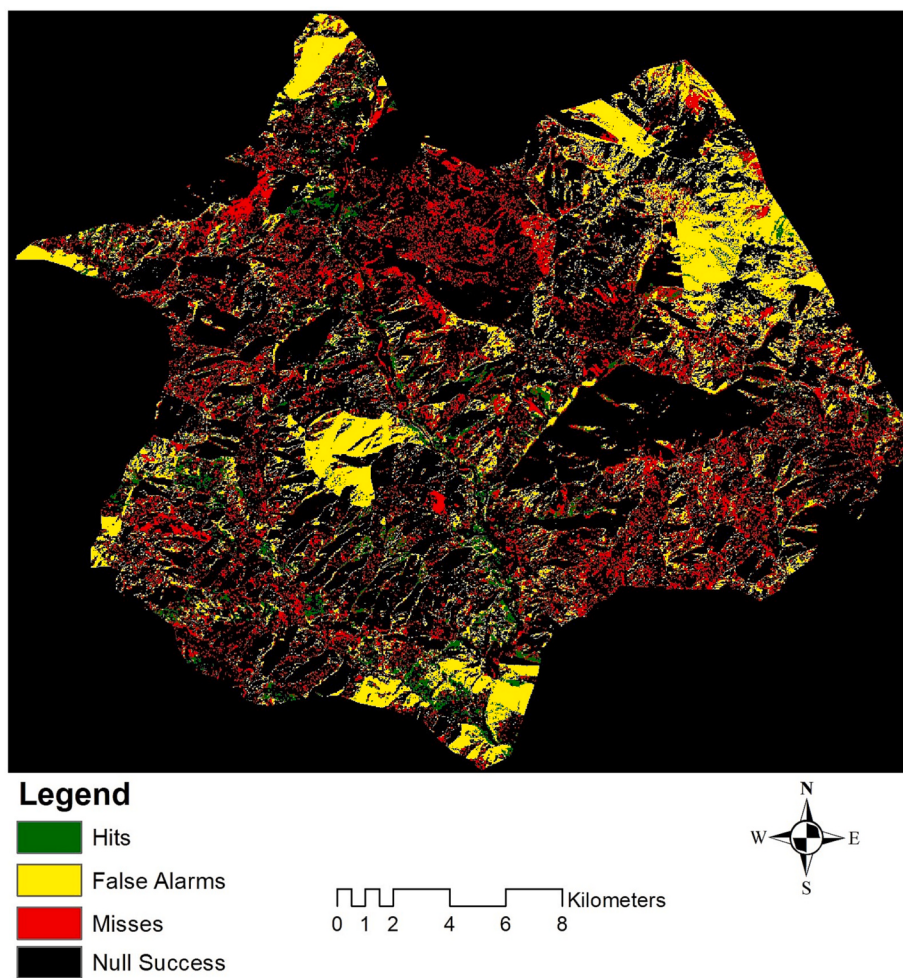


Fig. A.2. Visual validation-Figure of Merit (FOM) generated from LCM module in IDRISI Selva using 2008 (reference), 2020 (reference) and 2020 (simulated) LULC maps.

Table A.1
Possible ranges of Cohen's kappa (k).

S/N	Value range of kappa	Strength of agreement	% of reliability
1.	$k \leq 0$	No agreement	0–4%
2.	$0.01 \leq k \leq 0.20$	Fair	5–15%
3.	$0.21 \leq k \leq 0.40$	Slight	16–35%
4.	$0.41 \leq k \leq 0.60$	Moderate	36–63%
5.	$0.61 \leq k \leq 0.80$	Substantial	64–81%
6.	$0.81 \leq k \leq 1.00$	Almost perfect agreement	82–100%

References

- Abd El-Hamid, H.T., Hafiz, M.A., 2022. Modeling of carbon sequestration with land use and land cover in the northeastern part of the Nile Delta, Egypt. Arab. J. Geosci. 15 <https://doi.org/10.1007/s12517-022-10462-2>.
- Adelisardou, F., Zhao, W., Chow, R., Mederly, P., Minkina, T., Schou, J.S., 2022. Spatiotemporal change detection of carbon storage and sequestration in an arid ecosystem by integrating Google Earth engine and InVEST (the Jiroft plain, Iran). Int. J. Environ. Sci. Technol. 19, 5929–5944. <https://doi.org/10.1007/s13762-021-03676-6>.
- Adhikari, B.S., 2009. Status and distribution pattern of coarse woody debris along an altitudinal gradient in askot Wildlife Sanctuary, Uttarakhand, West Himalaya. J. For. Res. 20, 205–212. <https://doi.org/10.1007/s11676-009-0040-0>.
- Akash, Navneet, Bhandari, B.S., Bijlwan, K., 2022. Vulnerability of forest vegetation due to anthropogenic disturbances in Western Himalayan Region of India. In: Research Anthology on Ecosystem Conservation and Preserving Biodiversity. IGI Global, pp. 1297–1312. <https://doi.org/10.4018/978-1-6684-5678-1.CH062>.
- Alla, H., Moumoun, L., Balouki, Y., 2021. A multilayer perceptron neural network with selective-data training for flight arrival delay prediction. Sci. Program. Some 2021.
- Arsanjani, J.J., Helbich, M., Kainz, W., Boloorani, A.D., 2013. Integration of logistic regression, Markov chain and cellular automata models to simulate urban expansion. Int. J. Appl. Earth Obs. Geoinf. 21, 265–275. <https://doi.org/10.1016/j.jag.2011.12.014>.
- Asadi, M., Oshnooei-nooshabadi, A., Saleh, S., Sarafraz-asbagh, S., 2022. Simulation of Urban Sprawl by Comparison Cellular Automata-Markov and ANN, pp. 1–14. <https://doi.org/10.20944/preprints202208.0119.v1>.
- Avtar, R., Rinamalo, A.V., Umarhadi, D.A., Gupta, A., Khedher, K.M., Yunus, A.P., Singh, B.P., Kumar, P., Sahu, N., Sakti, A.D., 2022. Land use change and prediction for valuating carbon sequestration in Viti Levu Island, Fiji. Land 11. <https://doi.org/10.3390/land11081274>.
- Barbar, D., Areendran, G., Sahana, M., Sarma, K., Raj, K., Sivadas, A., 2021. Assessment and prediction of carbon sequestration using Markov chain and InVEST model in Sariska Tiger Reserve, India. J. Clean. Prod. 278 <https://doi.org/10.1016/j.jclepro.2020.123333>.

- Band, S.S., Janizadeh, S., Pal, S.C., Saha, A., Chakraborty, R., Shokri, M., Mosavi, A., 2020. Novel ensemble approach of deep learning neural network (DLNN) model and particle swarm optimization (PSO) algorithm for prediction of gully Erosion susceptibility. *Sensors* 20, 5609. <https://doi.org/10.3390/s20195609>.
- Bargali, H., Kumar, A., Singh, P., 2022. Plant studies in Uttarakhand, Western Himalaya—a comprehensive review. *Trees People* 8. <https://doi.org/10.1016/j.tfp.2022.100203>.
- Barnett, T.P., Adam, J.C., Lettenmaier, D.P., 2005. Potential impacts of a warming climate on water availability in snow-dominated regions. *Nat.* 438, 303–309. <https://doi.org/10.1038/nature04141>.
- Bera, B., Bhattacharjee, S., Sengupta, N., Shit, P.K., Adhikary, P.P., Sengupta, D., Saha, S., 2022. Significant reduction of carbon stocks and changes of ecosystem service valuation of Indian Sundarban. *Sci. Rep.* 12, 1–17. <https://doi.org/10.1038/s41598-022-11716-5>.
- Berooh, M., Briak, H., Cherif, E.K., Boulahfa, I., Ouallali, A., Mrabet, R., Kebede, F., Bernardino, A., Aboumaria, K., 2023. Future scenarios of land use / land cover (LULC) based on a CA-Markov simulation model: case of a Mediterranean watershed in Morocco. *Remote Sens.* 15 <https://doi.org/10.3390/rs15041162>.
- Bisht, S., Bargali, S.S., Bargali, K., Rawat, G.S., Rawat, Y.S., Fartyal, A., 2022. Influence of anthropogenic activities on Forest carbon stocks—a case study from Gorai Valley, Western Himalaya. *Sustain.* 14 <https://doi.org/10.3390/su142416918>.
- Bisht, S., Rawat, G.S., Bargali, S.S., Rawat, Y.S., Mehta, A., 2023. Forest vegetation response to anthropogenic pressures: a case study from Askot Wildlife Sanctuary, Western Himalaya. *Environ. Dev. Sustain.* <https://doi.org/10.1007/s10668-023-03130-2>.
- Camacho Olmedo, M.T., Paegelow, M., Mas, J.F., 2013. Interest in intermediate soft-classified maps in land change model validation: suitability versus transition potential. *Int. J. Geogr. Inf. Sci.* 27, 2343–2361. <https://doi.org/10.1080/13658816.2013.831867>.
- Choudhari, D.K., 2013. *Uncertainty Modeling for Asynchronous Time Series Data with Incorporation of Spatial Variation for Land Use/Land Cover Change*. University of Twente, Enschede, The Netherlands.
- Chu, X., Zhan, J., Li, Z., Zhang, F., Qi, W., 2019. Assessment on forest carbon sequestration in the three-north shelterbelt program region, China. *J. Clean. Prod.* 215, 382–389. <https://doi.org/10.1016/j.jclepro.2018.12.296>.
- Daman Singh, R., Gumber, S., Joshi, H., Singh, S.P., 2022. Allocation to tree bark in pine and oak species in fire affected mixed forests across the northern hemisphere. *For. Ecol. Manag.* 509, 120081 <https://doi.org/10.1016/J.FORECO.2022.120081>.
- Dangwal, B., Rana, S.K., Negi, V.S., Bhatt, I.D., 2022. Forest restoration enhances plant diversity and carbon stock in the sub-tropical forests of western Himalaya. *Trees People* 7, 100201. <https://doi.org/10.1016/j.tfp.2022.100201>.
- Faichia, C., Tong, Z., Zhang, J., Liu, X., Kazuva, E., Ullah, K., Al-Shaibah, B., 2020. Using RS data-based CA-Markov model for dynamic simulation of historical and future LUCC in Vientiane. *Laos. Sustain.* 12, 8410. <https://doi.org/10.3390/SU12208410>.
- Fernandes, M.M., de Fernandes, M.R.M., Garcia, J.R., Matricardi, E.A.T., de Almeida, A.Q., Pinto, A.S., Menezes, R.S.C., de Silva, A.J., de Lima, A.H.S., 2020. Assessment of land use and land cover changes and valuation of carbon stocks in the Sergipe semi-arid region, Brazil: 1992–2030. *Land Use Policy* 99, 104795. <https://doi.org/10.1016/j.landusepol.2020.104795>.
- FSI, 2019. *India State of Forest Report 2019*.
- Gebresellase, S.H., Wu, Z., Xu, H., Muhammed, W.I., 2023. Scenario-based LULC dynamics projection using the CA – Markov model on upper Awash Basin (UAB), Ethiopia. *Sustainability* 15. <https://doi.org/10.3390/su15021683>.
- Guo, D., Zhao, Z., Tan, J., 2019. Dynamic simulation of land use change based on logistic-CA-Markov and WLCA-CA-Markov models: a case study in three gorges reservoir area of Chongqing, China. *Environ. Sci. Pollut. Res.* 26, 20669–20688. <https://doi.org/10.1007/s11356-019-05127-9/TABLES/5>.
- Gupta, S., Remote, N., Centre, S., Anand, S., Singh, S., 2017. Valuation of carbon sequestration in Bidalna microwatershed, Uttarakhand, India using InVEST model. *Int. J. Adv. Earth Environ. Sci.* 5, 10–15. <https://doi.org/10.13140/RG.2.2.29675.90404>.
- Harris, N.L., Gibbs, D.A., Baccini, A., Birdsey, R.A., de Bruin, S., Farina, M., Fatoyinbo, L., Hansen, M.C., Herold, M., Houghton, R.A., Potapov, P.V., Suarez, D.R., Roman-Cuesta, R.M., Saatchi, S.S., Slay, C.M., Turubanova, S.A., Tyukavina, A., 2021. Global maps of twenty-first century forest carbon fluxes. *Nat. Clim. Chang.* 11, 234–240. <https://doi.org/10.1038/s41558-020-00976-6>.
- Hegde, N.P., Muralikrishna, I.V., Chalapatirao, K.V., 2007. *Integration of cellular automata and Gis for simulating land use changes*. 5th Int. Symp. Spat. Data Qual. - ISPRS 1, 1–2.
- Hoque, M.Z., Cui, S., Islam, I., Xu, L., Ding, S., 2021. Dynamics of plantation forest development and ecosystem carbon storage change in coastal Bangladesh. *Ecol. Indic.* 130, 107954 <https://doi.org/10.1016/j.ecolind.2021.107954>.
- Hua, A.K., 2017. Application of Ca-Markov model and land use / land cover changes in Malacca river watershed. *Appl. Ecol. Environ. Res.* 15, 605–622. <https://doi.org/10.15666/aeer/1504.605622>.
- Itami, R.M., 1994. Simulating spatial dynamics: cellular automata theory. *Landsc. Urban Plan.* 30, 27–47. [https://doi.org/10.1016/0169-2046\(94\)90065-5](https://doi.org/10.1016/0169-2046(94)90065-5).
- IUCN, 2021. *Issues Brief: Forest and Climate Change*.
- Kangas, J., Ollikainen, M., 2022. A PES scheme promoting forest biodiversity and carbon sequestration. *Forest Policy Econ.* 136, 102692 <https://doi.org/10.1016/J.FORPOL.2022.102692>.
- Katila, M., Puustjärvi, E., 2003. *Impact of New Markets for Environmental Services on Forest Products Trade*. INDUFOR.
- Kaur, S., Babbar, D., Sarif, O., Ghatak, A., Jaafari, A., 2022. Assessment of carbon sequestration using InVEST model in Delhi, India. In: Conservation, Management and Monitoring of Forest Resources in India, pp. 33–56. https://doi.org/10.1007/978-3-030-98233-1_2.
- Khawaldah, H.A., Farhan, I., Alzoubi, N.M., 2020. Simulation and prediction of land use and land cover change using GIS, remote sensing and CA-Markov model. *Glob. J. Environ. Sci. Manag.* 6, 215–232. <https://doi.org/10.22034/gjesm.2020.02.07>.
- Kou, J., Wang, J., Ding, J., Ge, X., 2023. Spatial simulation and prediction of land use/land cover in the transnational Ili-Balkhash Basin. *Remote Sens.* 15 <https://doi.org/10.3390/rs15123059>.
- Kumar, V., Agrawal, S., 2022. Urban modelling and forecasting of landuse using SLEUTH model. *Int. J. Environ. Sci. Technol.* <https://doi.org/10.1007/s13762-022-04331-4>.
- Kumar, V., Agrawal, S., 2023. A multi - layer perceptron – Markov chain based LULC change analysis and prediction using remote sensing data in Prayagraj district, India. *Environ. Monit. Assess.* <https://doi.org/10.1007/s10661-023-11205-w>.
- Kumar, N., Singh, V.G., Singh, S.K., Behera, D.K., Gašparović, M., 2023. Modeling of land use change under the recent climate projections of CMIP6: a case study of Indian river basin. *Environ. Sci. Pollut. Res.* 30, 107219–107235. <https://doi.org/10.1007/s11356-023-26960-z>.
- Leta, M.K., Demissie, T.A., Tränckner, J., 2021. Modeling and prediction of land use land cover change dynamics based on land change modeler (lcm) in nashe watershed, upper Blue Nile basin, Ethiopia. *Sustain.* 13 <https://doi.org/10.3390/su13073740>.
- Liang, Y., Liu, L., Huang, J., 2017. Integrating the SD-CLUE-S and InVEST models into assessment of oasis carbon storage in northwestern China. *PLoS One* 12, 1–15. <https://doi.org/10.1371/journal.pone.0172494>.
- Liang, X., Liu, X., Li, X., Chen, Y., Tian, H., Yao, Y., 2018. Landscape and urban planning delineating multi-scenario urban growth boundaries with a CA-based FLUS model and morphological method. *Landsc. Urban Plan.* 177, 47–63. <https://doi.org/10.1016/j.landurbplan.2018.04.016>.
- Mahfuz, F., 2021. *Markov Chains and their Applications*. University of Texas at Tyler.
- Mansourian, S., Belokurov, A., Stephenson, P.J., 2009. The role of forest protected areas in adaptation to climate change. *Unasylva* 60, 63–69.
- Marko, K., Zulkarnain, F., Kusratmoko, E., 2016. Coupling of Markov chains and cellular automata spatial models to predict land cover changes (case study: upper ci Leungsii catchment area). *IOP Conf. Ser. Earth Environ. Sci.* 47 <https://doi.org/10.1088/1755-1315/47/1/012032>.
- Mirici, M.E., Berberoglu, S., Akin, A., Satir, O., 2017. Land use/cover change modelling in a Mediterranean rural landscape using multi-layer perceptron and Markov chain (MLP-mc). *Appl. Ecol. Environ. Res.* 467–486 https://doi.org/10.15666/aeer/1601_467486.
- Miteva, D.A., Pattanayak, S.K., Ferraro, P.J., 2012. Evaluation of biodiversity policy instruments: what works and what doesn't? *Oxf. Rev. Econ. Policy* 28, 69–92. <https://doi.org/10.1093/OXREP/GRS009>.
- MoEFCC, 2018. *National REDD+ Strategy INDIA*. Minist. Environ. For. Clim. Chang. Gov. India.
- Momo, N., Devi, T.T., 2022. Assessment of land surface temperature and carbon sequestration using remotely sensed satellite data in the Imphal-west district, Manipur, India. *J. Earth Syst. Sci.* 131 <https://doi.org/10.1007/s12040-022-01944-8>.
- Moritz, R.E., Gawel, A., 2021. *Increasing Climate Ambition: Analysis of an International Carbon Price Floor*. World Economic Forum, Geneva, Switzerland.
- Naime, J., Mora, F., Sánchez-Martínez, M., Arreola, F., Balvanera, P., 2020. Economic valuation of ecosystem services from secondary tropical forests: trade-offs and implications for policy making. *For. Ecol. Manag.* 473, 118294 <https://doi.org/10.1016/j.foreco.2020.118294>.
- Nasiri, V., Darvishsefat, A.A., Rafiee, R., Shirvany, A., Hemat, M.A., 2019. Land use change modeling through an integrated multi-layer perceptron neural network and Markov chain analysis (case study: Arasbaran region, Iran). *J. For. Res.* 30, 943–957. <https://doi.org/10.1007/s11676-018-0659-9>.
- Nath, B., Wang, Z., Ge, Y., Islam, K., Singh, R.P., Niu, Z., 2020. Land use and land cover change modeling and future potential landscape risk assessment using Markov-CA model and analytical hierarchy process. *ISPRS Int. J. Geo-Inform.* 9 <https://doi.org/10.3390/ijgi9020134>.
- Natural Capital Project, 2022. InVEST User Guide — InVEST Documentation [WWW Document]. URL: <http://releases.naturalcapitalproject.org/invest-userguide/1atest/en/index.html> (accessed 5.29.23).
- Negi, G., 2018. Forestry and biodiversity conservation research in the Indian Himalayan forestry and biodiversity conservation research in the Indian Himalayan region: emerging concepts. *Environ. Anal. Ecol. Stud.* 3, 1–6. <https://doi.org/10.31031/EAES.2018.0000564>.
- Nguyen, M.D., Ancev, T., Randall, A., 2020. Forest governance and economic values of forest ecosystem services in Vietnam. *Land Use Policy* 97, 1–17. <https://doi.org/10.1016/j.landusepol.2018.03.028>.
- OECD, 2022. *Pricing Greenhouse Gas Emissions: Key Findings for India*.
- Omar, N.Q., Ahamad, M.S.S., Wan Hussin, W.M.A., Samat, N., Binti Ahmad, S.Z., 2014. Markov CA, multi regression, and multiple decision making for modeling historical changes in Kirkuk City, Iraq. *J. Indian Soc. Remote Sens.* 42, 165–178. <https://doi.org/10.1007/S12524-013-0311-2/TABLES/6>.
- Omasa, K., Qiu, G.Y., Watanuki, K., Yoshimi, K., Akiyama, Y., 2003. Accurate estimation of Forest carbon stocks by 3-D Remote sensing of individual trees. *Environ. Sci. Technol.* 37, 1198–1201. <https://doi.org/10.1021/ES0259887>.
- Ouyang, Z., Zheng, H., Xiao, Y., Polasky, S., Liu, J., Xu, W., Wang, Q., Zhang, L., Xiao, Yang, E., Jiang, L., Lu, F., Wang, X., Yang, G., Gong, S., Wu, B., Zeng, Y., Yang, W., Daily, G.C., 2016. Improvements in ecosystem services from investments in natural capital. *Ecosyst. Serv.* 352, 1455–1459. https://doi.org/10.1126/SCIENCE.AAF2295/SUPPL_FILE/AAF2295_OUYANG.SM.PDF.

- Pache, R.G., Abrudan, I.V., Niță, M.D., 2021. Economic valuation of carbon storage and sequestration in Retezat National Park, Romania. *Forests*. <https://doi.org/10.3390/f12010043>.
- Piyathilake, I.D.U.H., Udayakumara, E.P.N., Ranaweera, L.V., Gunatilake, S.K., 2022. Modeling predictive assessment of carbon storage using InVEST model in Uva province, Sri Lanka. *Model. Earth Syst. Environ.* 8, 2213–2223. <https://doi.org/10.1007/s40808-021-01207-3>.
- Pontius, R.G., Boersma, W., Castella, J.C., Clarke, K., Nijs, T., Dietzel, C., Duan, Z., Fotsing, E., Goldstein, N., Kok, K., Koomen, E., Lippitt, C.D., McConnell, W., Mohd Sood, A., Pijanowski, B., Pithadia, S., Sweeney, S., Trung, T.N., Veldkamp, A.T., Verburg, P.H., 2008. Comparing the input, output, and validation maps for several models of land change. *Ann. Reg. Sci.* 42, 11–37. <https://doi.org/10.1007/s00168-007-0138-2>.
- Rajbanshi, J., Das, S., 2021. Changes in carbon stocks and its economic valuation under a changing land use pattern—a multitemporal study in Konar catchment, India. *L. Degrad. Dev.* 32, 3573–3587. <https://doi.org/10.1002/lrd.3959>.
- Rawal, R.S., Dhar, U., 2001. Protected area network in Indian Himalayan region: need for recognizing values of low profile protected areas. *Curr. Sci.* 81, 175–184.
- Rawal, R., Negi, V.S., Bhatt, I.D., 2021. Changing outlook on harnessing biodiversity values – a special focus on Indian Himalaya. *J. Graph. Era Univ.* 9, 55–82. <https://doi.org/10.13052/jgeu0975-1416.914>.
- Rawat, P.K., Sharma, A.K., 2012. Geo-diversity and its hydrological response in relation to landslide susceptibility in the Himalaya: a GIS-based case study. *Georisk* 6, 229–251. <https://doi.org/10.1080/17499518.2012.739701>.
- Ricke, K., Drouet, L., Caldeira, K., Tavoni, M., 2018. Country-level social cost of carbon. *Nat. Clim. Chang.* 8, 895–900. <https://doi.org/10.1038/s41558-018-0282-y>.
- Sabree Ali, A.H., Amany, A.K., Jalil, M.A., 2020. Predicting the future growth depending on GIS and IDRISI program, city of Najaf-Iraq. *IOP Conf. Ser. Mater. Sci. Eng.* 881 <https://doi.org/10.1088/1757-899X/881/1/012031>.
- Sagar, R., Raghubanshi, A.S., Singh, J.S., 2003. Tree species composition, dispersion and diversity along a disturbance gradient in a dry tropical forest region of India. *For. Ecol. Manag.* 186, 61–71. [https://doi.org/10.1016/S0378-1127\(03\)00235-4](https://doi.org/10.1016/S0378-1127(03)00235-4).
- Samant, S.S., Rawal, R.S., Dhar, U., 2006. Diversity, extraction and status of fodder species in Askot wildlife sanctuary, West Himalaya, India. *Int. J. Biodivers. Sci. Manag.* 2, 29–42. <https://doi.org/10.1080/17451590609618097>.
- Sedjo, R., Sohngen, B., 2012. Carbon sequestration in forests and soils. *Ann. Rev. Resour. Econ.* 4, 127–144. <https://doi.org/10.1146/annurev-resource-083110-115941>.
- Shafizadeh Moghadam, H., Helbich, M., 2013. Spatiotemporal urbanization processes in the megacity of Mumbai, India: a Markov chains-cellular automata urban growth model. *Appl. Geogr.* 40, 140–149. <https://doi.org/10.1016/j.apgeog.2013.01.009>.
- Shivakumar, B.R., Rajashekharadhy, S.V., 2018. Investigation on land cover mapping capability of maximum likelihood classifier: a case study on north Canara, India. *Procedia Comput. Sci.* 143, 579–586. <https://doi.org/10.1016/j.procs.2018.10.434>.
- Singh, S.P., 2007. Himalayan Forest Ecosystem Services Incorporating in National Accounting. Central Himalayan Environment Association (CHEA), Uttarakhand, India.
- Singh, S.K., Mustak, S., Srivastava, P.K., Szabó, S., Islam, T., 2015. Predicting spatial and decadal LULC changes through cellular automata Markov chain models using earth observation datasets and geo-information. *Environ. Process.* 2, 61–78. <https://doi.org/10.1007/s40710-015-0062-x>.
- Soares-Filho, B., Moutinho, P., Nepstad, D., Anderson, A., Rodrigues, H., Garcia, R., Dietzsch, L., Merry, F., Bowman, M., Hissa, L., Silvestrini, R., Maretti, C., 2010. Role of Brazilian Amazon protected areas in climate change mitigation. *Proc. Natl. Acad. Sci. U. S. A.* 107, 10821–10826. <https://doi.org/10.1073/pnas.0913048107>.
- Tao, Y., Tian, L., Wang, C., 2023. Dynamic simulation of land use and land cover and its effect on carbon storage in the Nanjing metropolitan circle under different development scenarios. *Front. Ecol. Evol.* 11, 1–16. <https://doi.org/10.3389/fevo.2023.1102015>.
- Tewari, V.P., Verma, R.K., von Gadow, K., 2017. Climate change effects in the Western Himalayan ecosystems of India: evidence and strategies. *For. Ecosyst.* 4 <https://doi.org/10.1186/s40663-017-0100-4>.
- Tolangay, D., Moktan, S., 2020. Trend of studies on carbon sequestration dynamics in the Himalaya hotspot region: a review. *J. Appl. Nat. Sci.* 12, 647–660. <https://doi.org/10.31018/jans.v12i4.2426>.
- Vass, M.M., Elofsson, K., 2016. Is forest carbon sequestration at the expense of bioenergy and forest products cost-efficient in EU climate policy to 2050? *J. For. Econ.* 24, 82–105. <https://doi.org/10.1016/j.jfe.2016.04.002>.
- Verma, P., Ghosh, P.K., 2023. The Economics of Forest Carbon Sequestration: A Bibliometric Analysis, Environment, Development and Sustainability. Springer, Netherlands. <https://doi.org/10.1007/s10668-023-02922-w>.
- Verma, P., Kumar Ghosh, P., 2022. REDD+ strategy for forest carbon sequestration in India. *Holist. Approach Environ.* 12, 117–130. <https://doi.org/10.33765/thate.12.3.4>.
- Vinayak, B., Lee, H.S., Shirishkumar, G., 2020. Prediction of land use land cover for 2050 in Mumbai City, India, using multi-layer perceptron neural network-based Markov chain model. *Sustainability* 13. <https://doi.org/10.3390/su13020471>.
- Wayburn, L.A., 2009. The role of forests in U.S. Climate policy. *L. Lines* 12, 2–7.
- Yu, Y., Li, J., Zhou, Z., Zeng, L., Zhang, C., 2020. Estimation of the value of ecosystem carbon sequestration services under different scenarios in the Central China (the Qinling-Daba mountain area). *Sustain.* 12, 1–18. <https://doi.org/10.3390/su12010337>.
- Zhang, T., Cheng, C., Wu, X., 2023. Mapping the spatial heterogeneity of global land use and land cover from 2020 to 2100 at a 1 km resolution. *Sci. Data* 10, 1–15. <https://doi.org/10.1038/s41597-023-02637-7>.